Tensile Ductility and Localized Fracture of AHSS

Xin Sun
Pacific Northwest National laboratory

Workshop for Addressing Key Technology Gaps in Implementing Advanced High-Strength Steels for Automotive Lightweighting

February 9, 2012

PNNL-SA-85780

Key Technology Gaps in Implementing 1st GEN Advanced High Strength Steel – Ductility and Localized Fracture

- Ductility under uniform loading:
  - Macroscopic phenomenological approach
  - Meso-scale microstructure based approach
- Fracture under localized loading:
  - Occurs in bending (especially under tension)
  - Edge stretching
  - Conventional FLD does not apply
  - Difficult to predict analytically

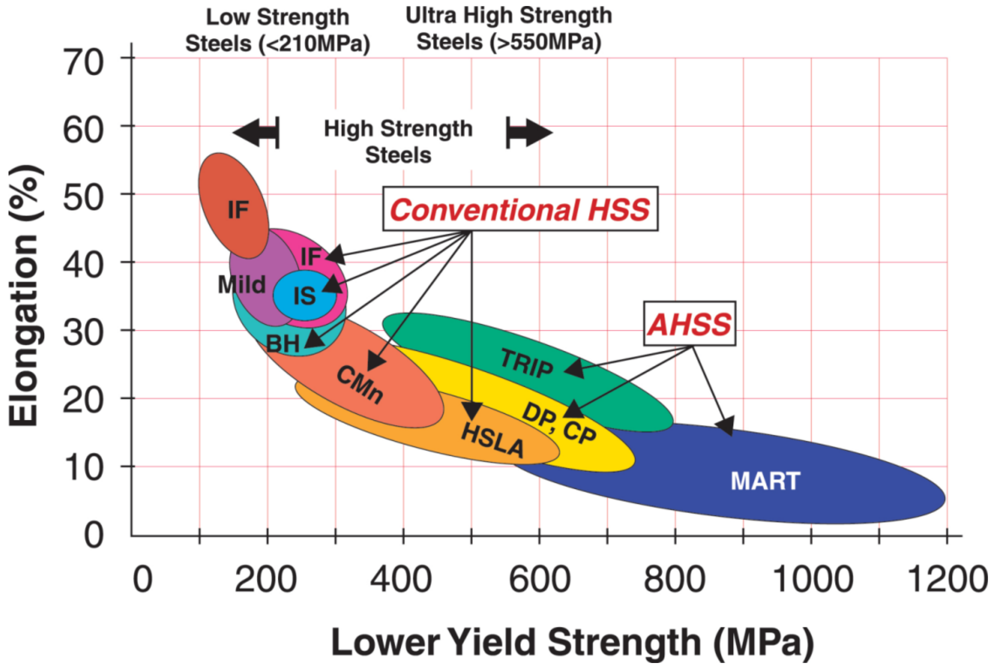

Northwest
ONAL LABORATORY
attelle Since 1965

MIT's fracture modeling framework

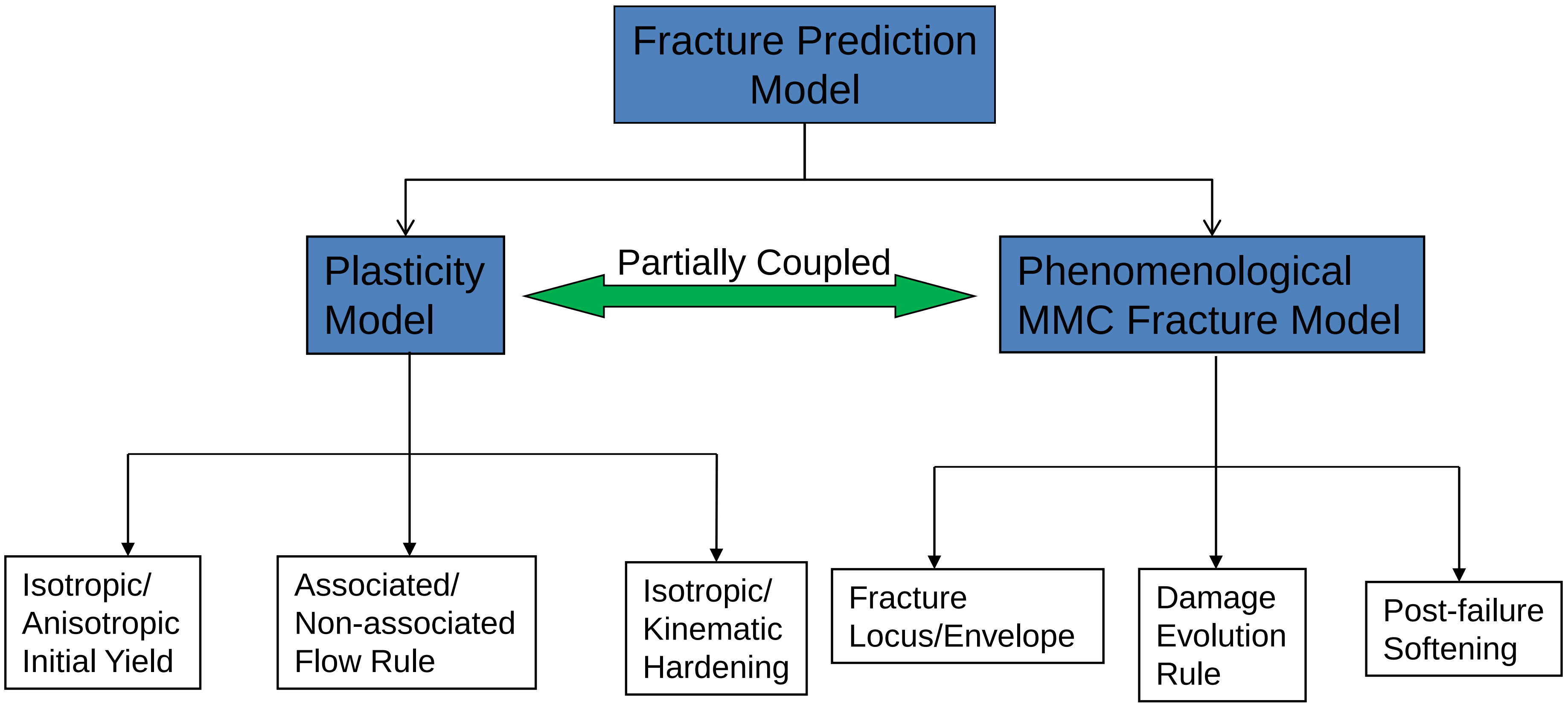

Fracture calibration tests

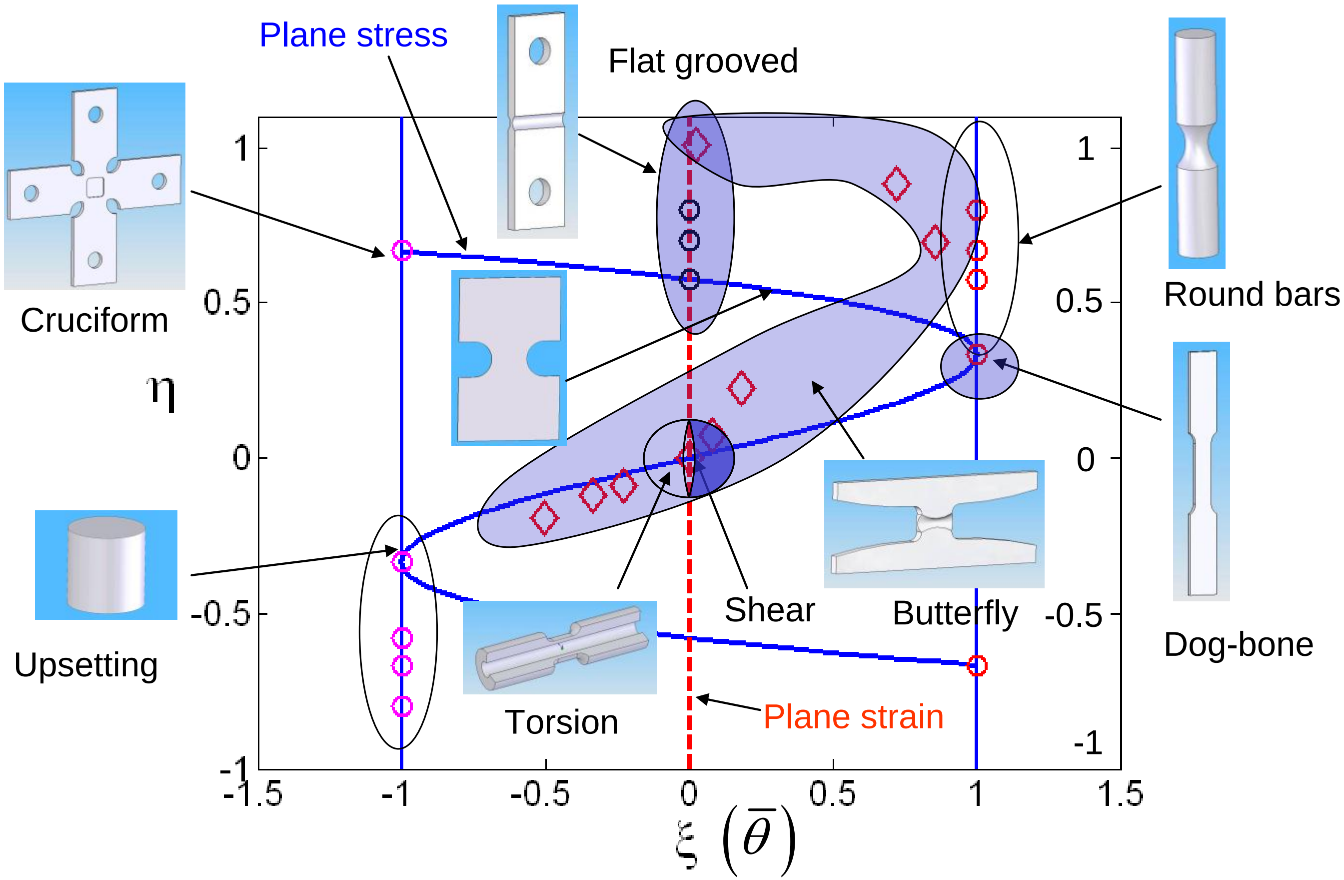

A complete representation of various stress states and ranges covered by various tests

Hybrid experimental-numerical calibration

Various types of fracture specimens

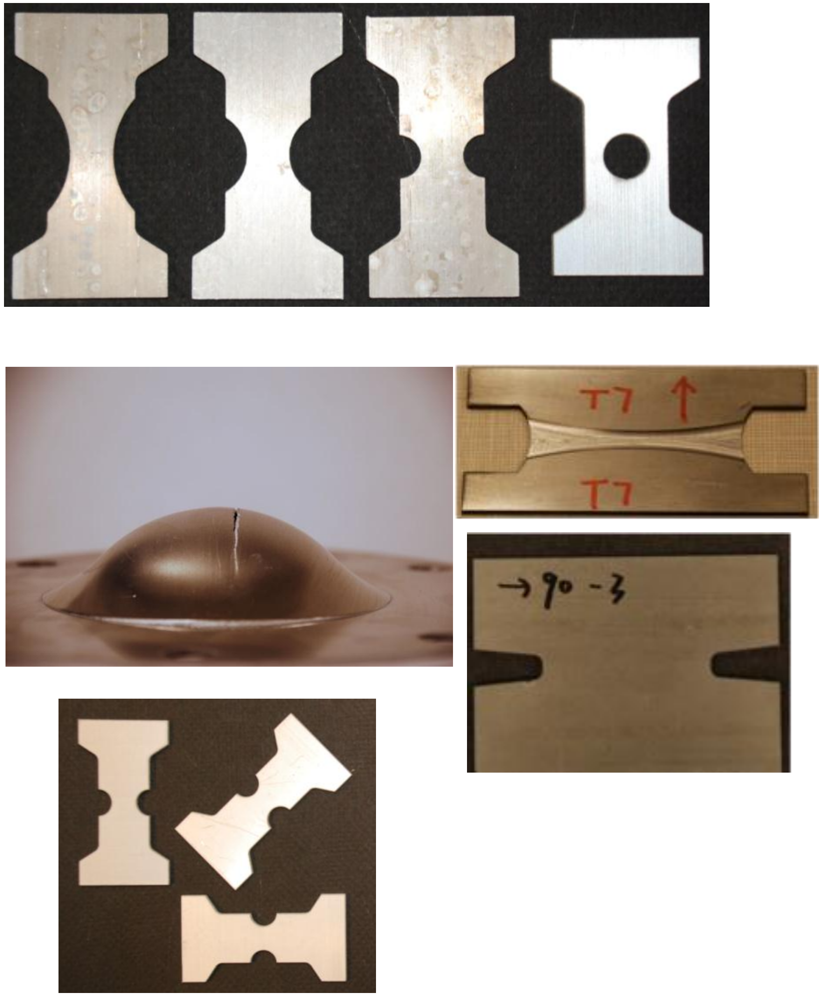

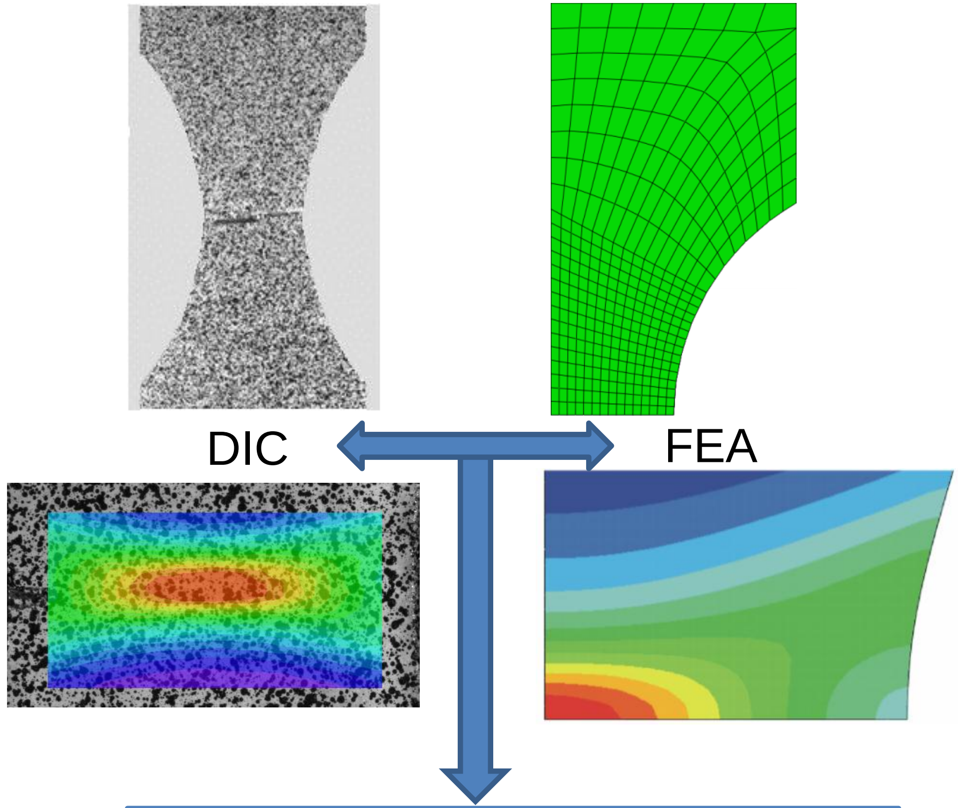

Careful correlation between experiments and FEA ensures accurate local strain and stress state evolution

Results: Fracture initiation location

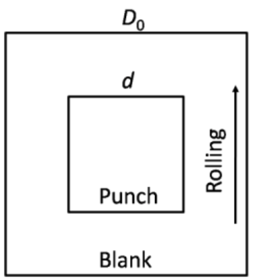

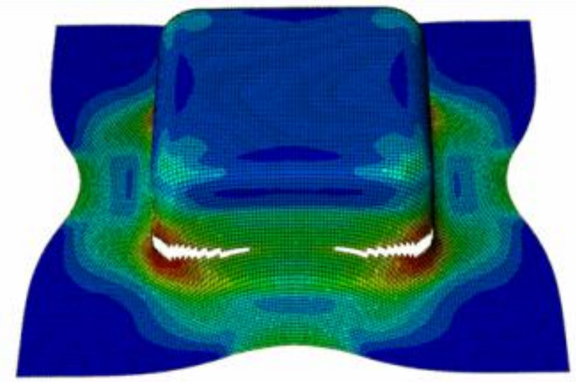

Square punch

Failure location shifting is accurately predicted.

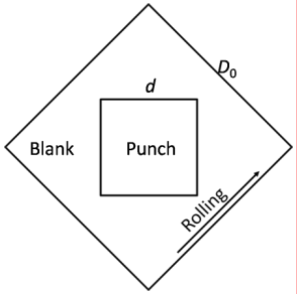

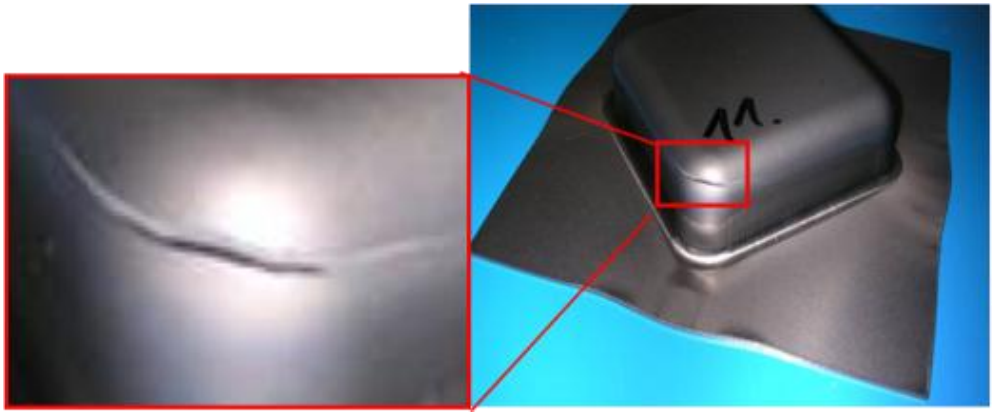

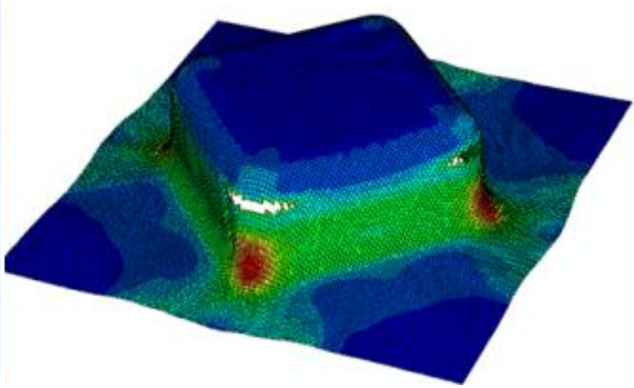

Predicting AHSS Ductility under Uniform Deformation – PNNL

- Microstructure based finite element analyses developed to predict tensile ductility and FLD of 1st Gen AHSS:
  - DP980:
    - Effects of martensite mechanical properties on behavior of DP980
    - Effects of martensite morphology on forming behavior of DP980
  - Effects of martensite volume fraction on DP steel properties:
    - Stress vs. strain behaviors
    - Failure driving force
  - TRIP800:
    - Transformation kinetics under different loading conditions simulated

Meso-Scale Finite Element Modeling of AHSS Based on Actual Microstructure

Actual Structure of DP980

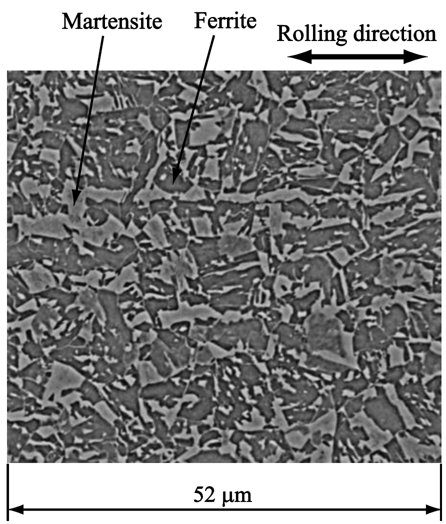

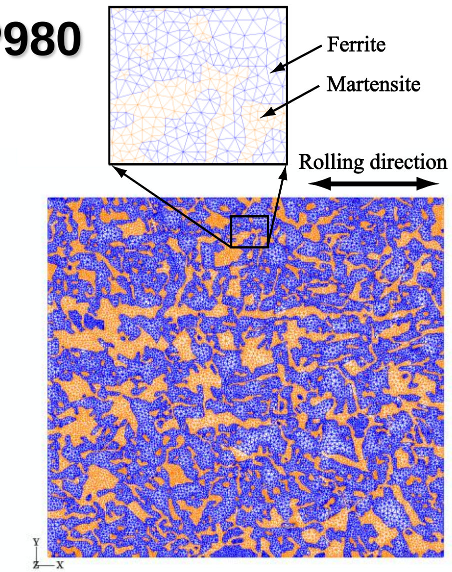

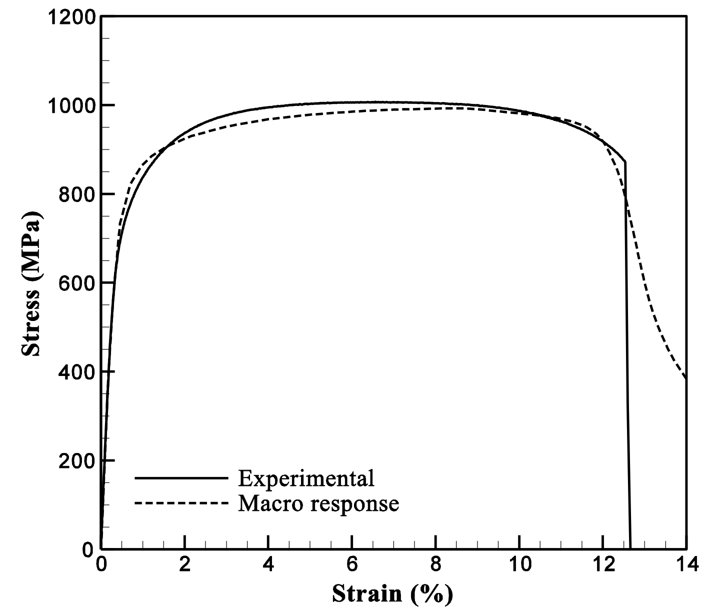

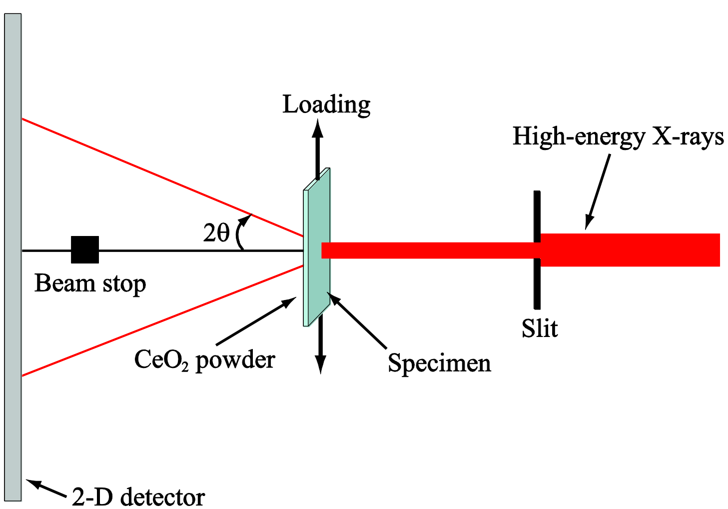

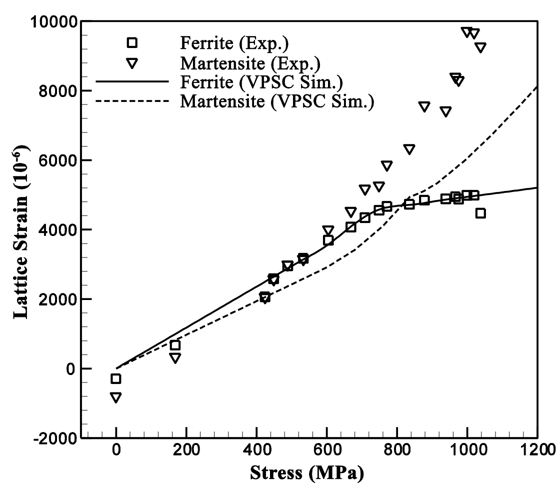

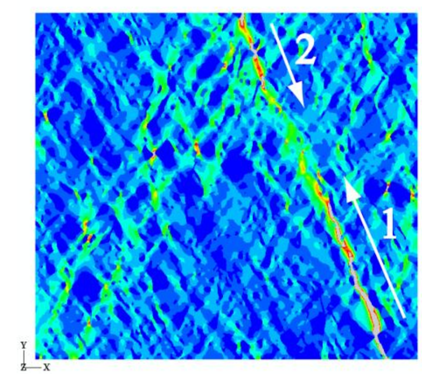

RVE in Fig. 4(b)

Effects of Loading Conditions on the Failure Mode

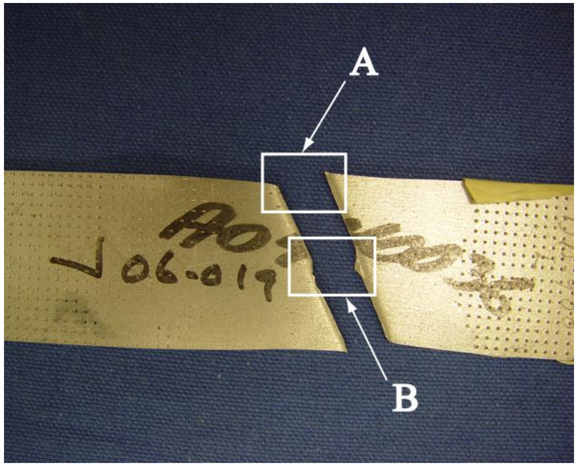

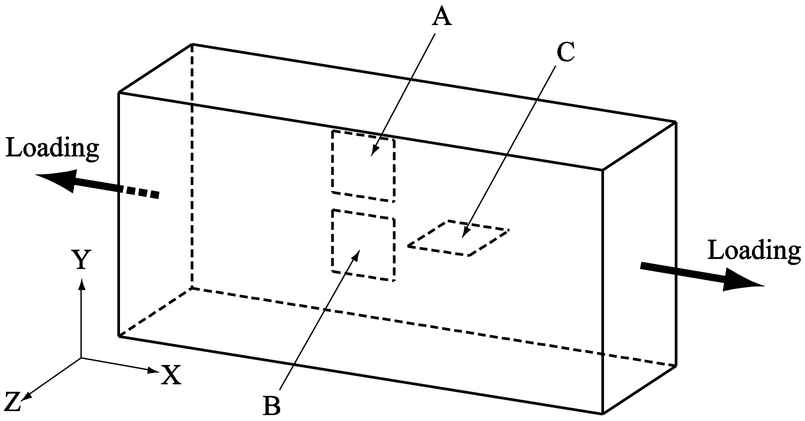

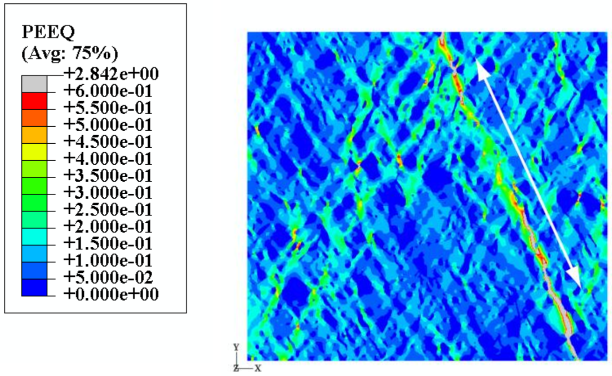

Case A – Free lateral edges

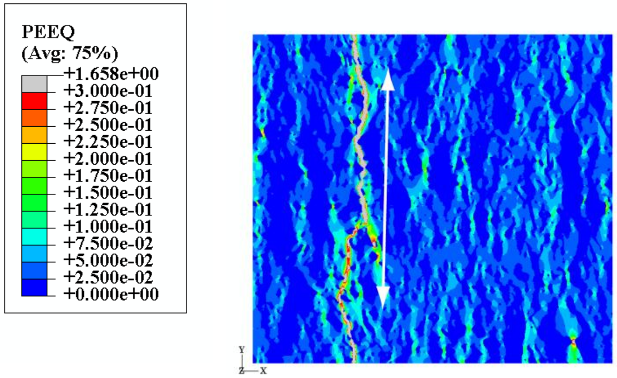

Case B – Constrained lateral edges

Sun et al, *Int. J. Plasticity*, 2009.

Effects of Martensite Mechanical Properties on Tensile Behavior of DP980

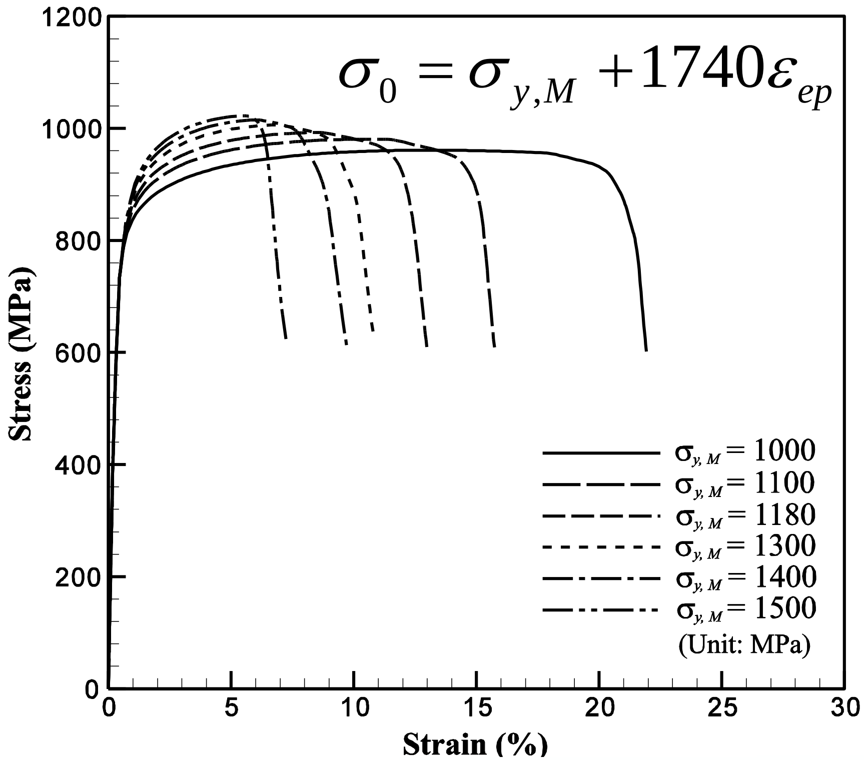

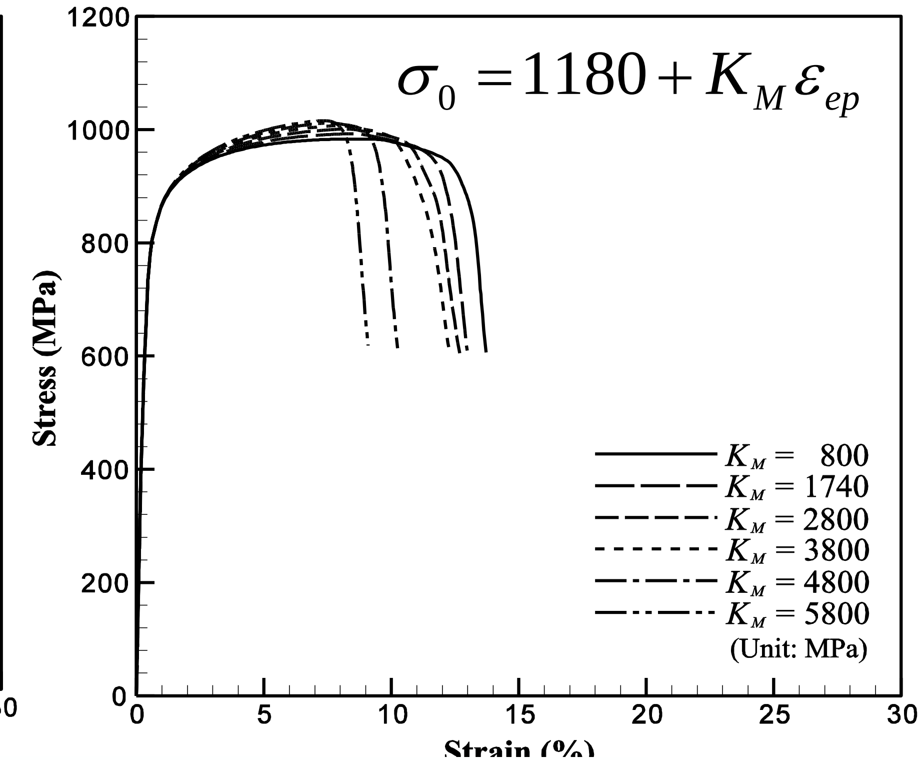

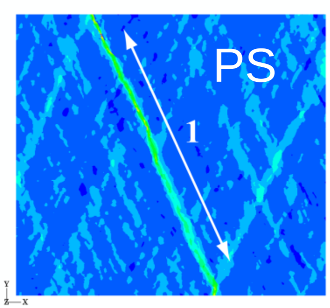

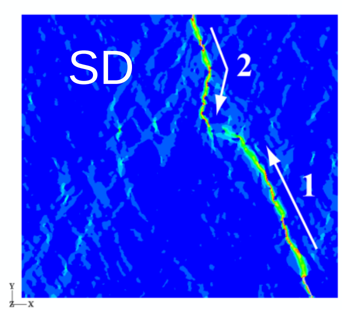

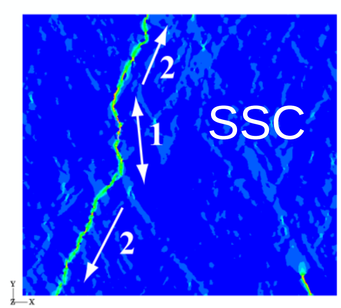

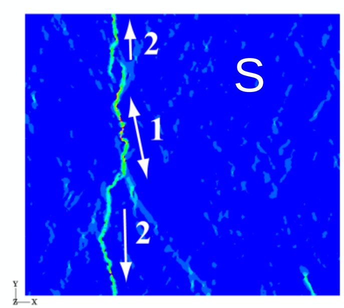

Choi et al., MMTA, 2009.

Effects of Martensite Volume Fraction and Ferrite Ductility on Ductility of DP Steels

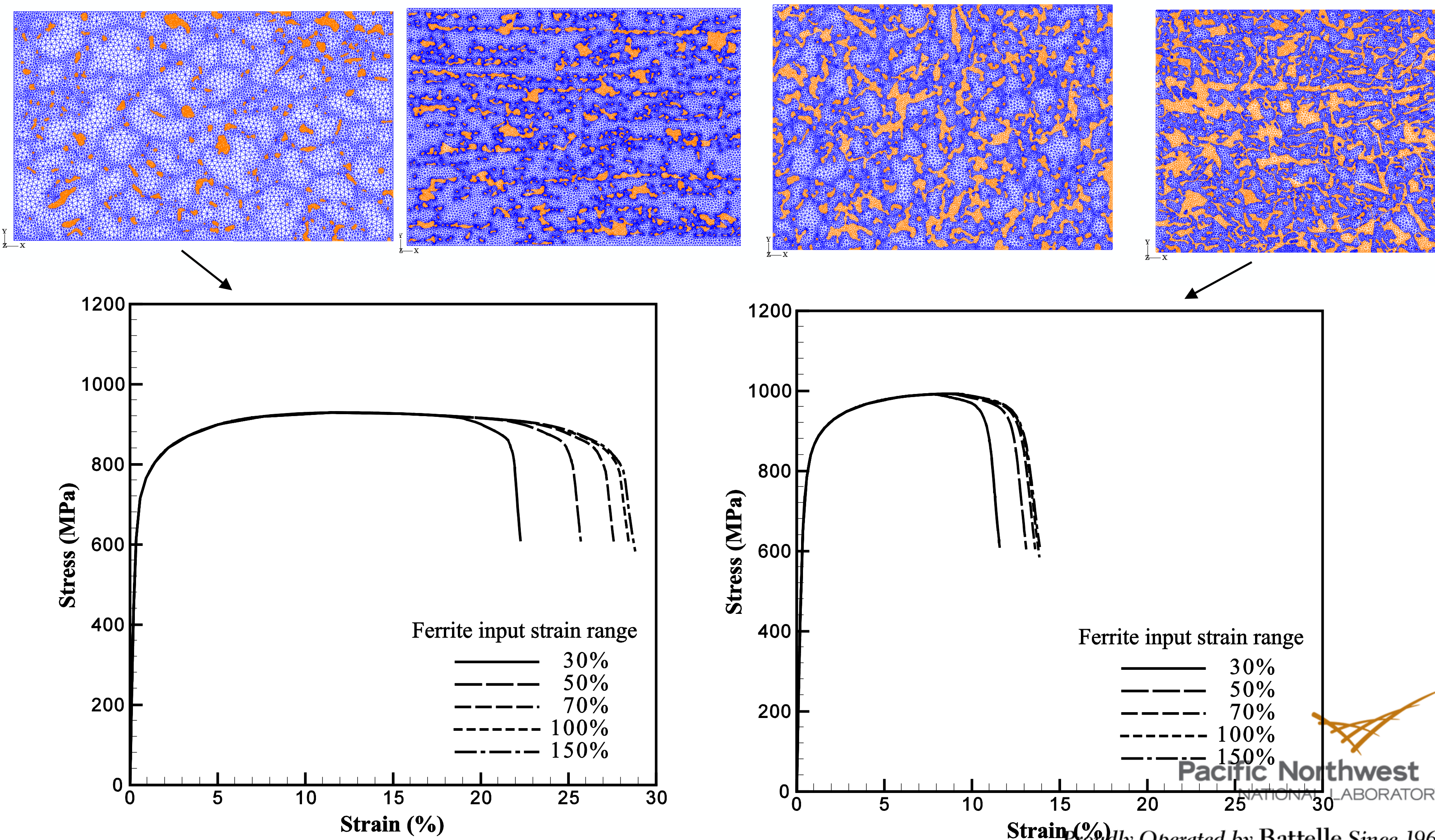

Effects of Martensite Volume Fraction and Voids on Failure of DP Steels

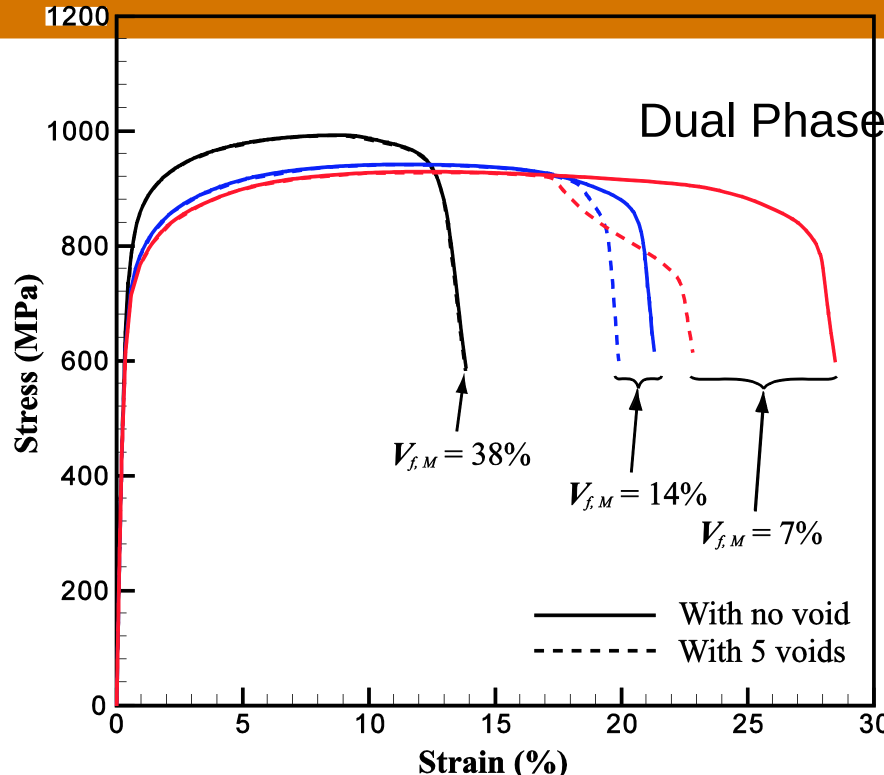

Sun et al, Mat. Sci. Eng. A, 2009.

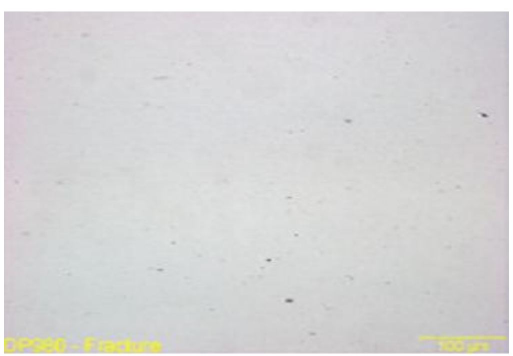

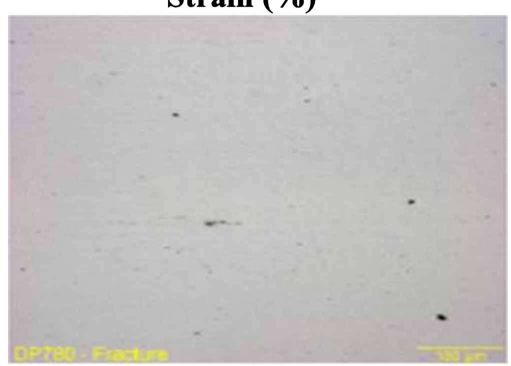

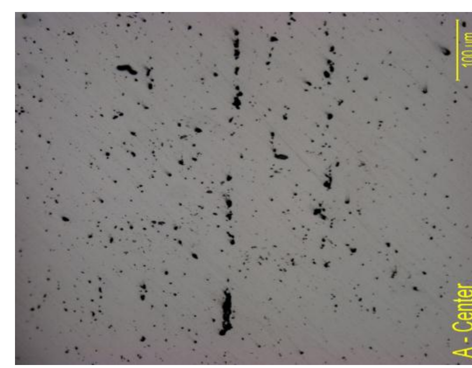

Micrographs from EWI's A/SP Shear Fracture Project Update 9-10-2008

TRIP800 – Modeling of Phase Transformation and Ultimate Ductility Under Different Loading Conditions

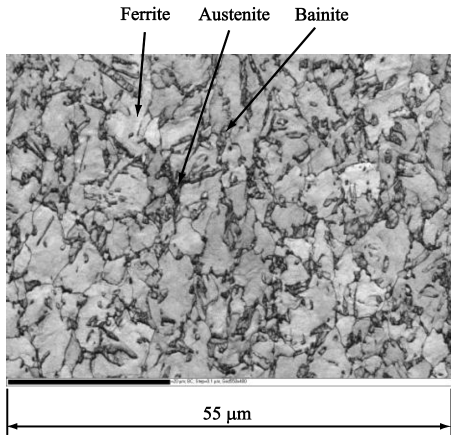

SEM picture

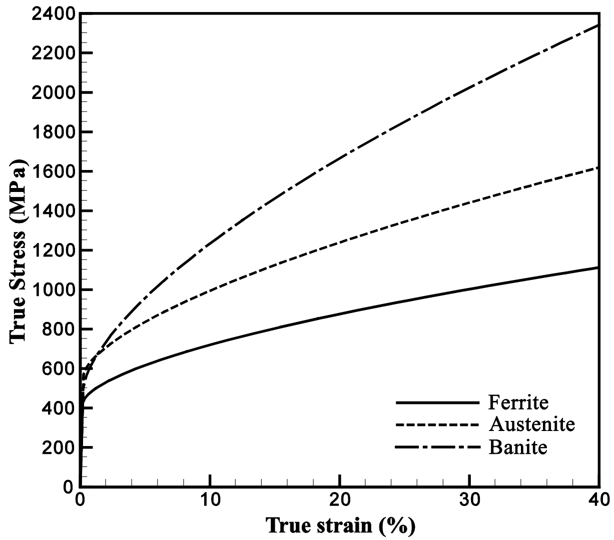

Phase properties from HEXRD

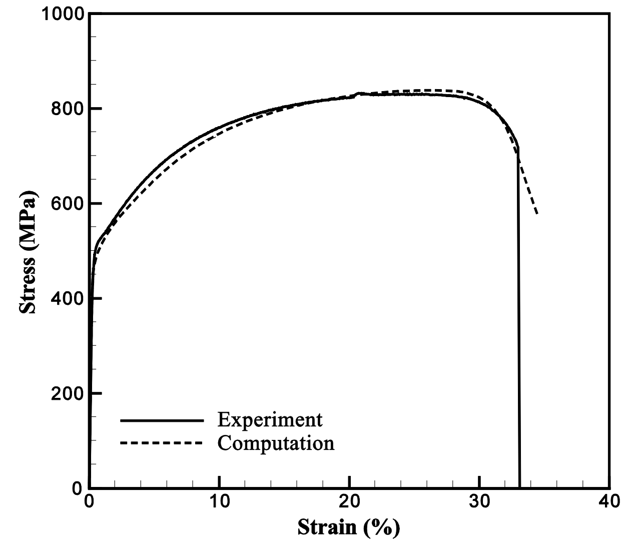

Overall response

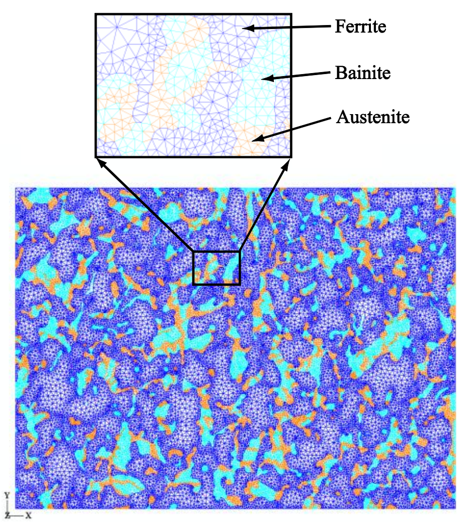

Microstructure-based RVE

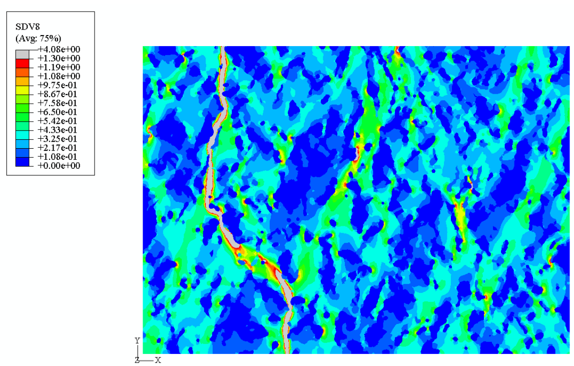

Failure mode (Split-type)

$$\Pi = R\sqrt{3J_2}\left[1 + k\frac{J_3}{J_2^{3/2}}\right] + \frac{\alpha I_1}{3}$$

Transformation yield function
Here, Πc =29MPa is used.

Choi, et al., *Acta Mater.*, 57, pp. 2592-2604, 2009.

Pacific Northwest
NATIONAL LABORATORY

Proudly Operated by Battelle *Since 1965*

Modeling of Phase Transformation and Ultimate Ductility for TRIP800 Under Different Loading Conditions

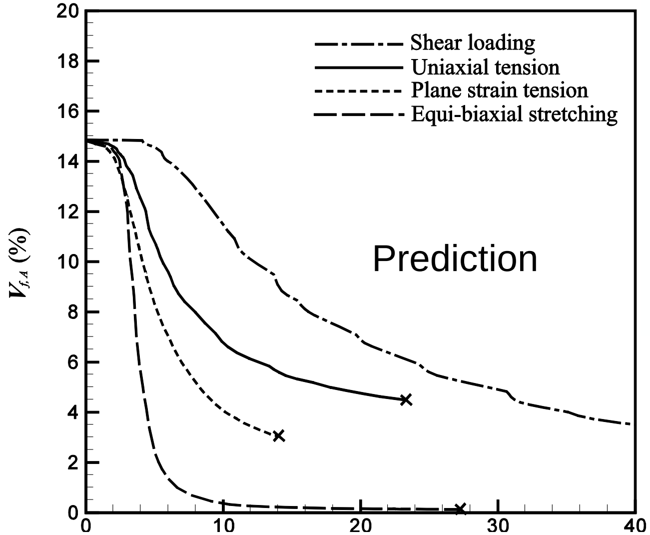

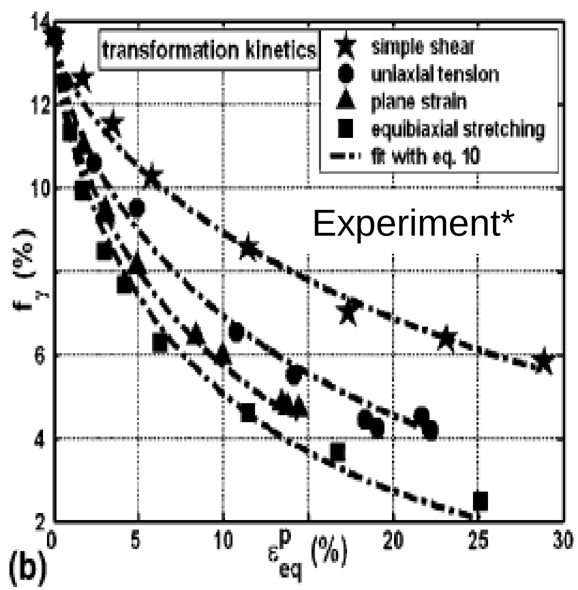

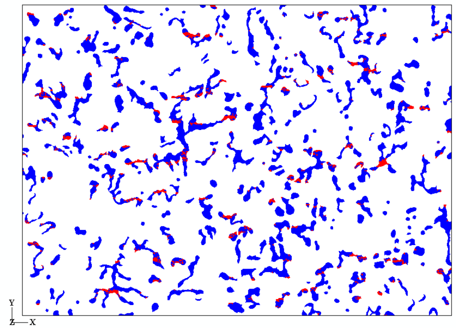

(a) Shear loading

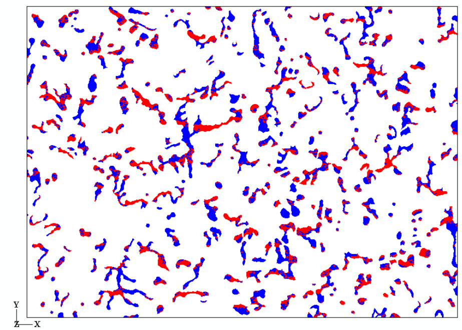

(b) Uniaxial tension

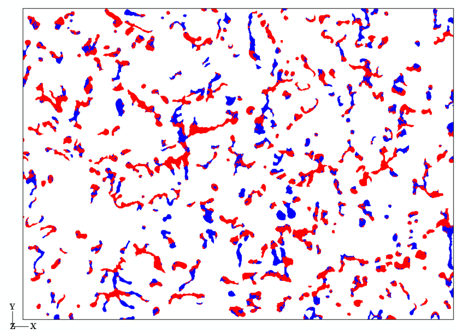

(c) Plane strain

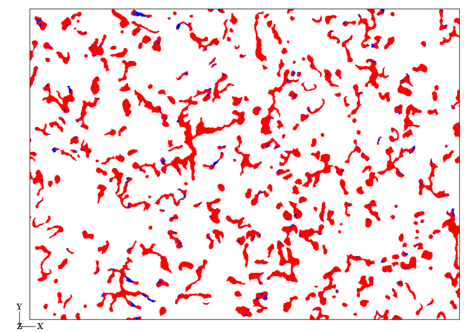

(d) Equi-biaxial stretching

Plotted at 7.7% strain

1. Predicted transformation kinetics and ultimate ductility (indicated by x) under different loading conditions are in qualitatively good agreements with experimental measurements.

•M. Radu et al. / Scripta Materialia 52 (2005) 525–530.
•KS. Choi, et al. Acta Mat. 57 (2009) 2592–2604.

Effects of Retained Austenite Stability on Ductility and Formability of TRIP800

- Critical value of Π_c was varied to investigate the influence of austenite stability.
- Higher austenite stability is beneficial in increasing the ductility of TRIP steels since it delays the martensitic transformation.
- In turn, improved ductility results in better formability.
- Improvement of formability can be more prominent than shown in the figure below, depending on the phase properties, microstructures, etc.

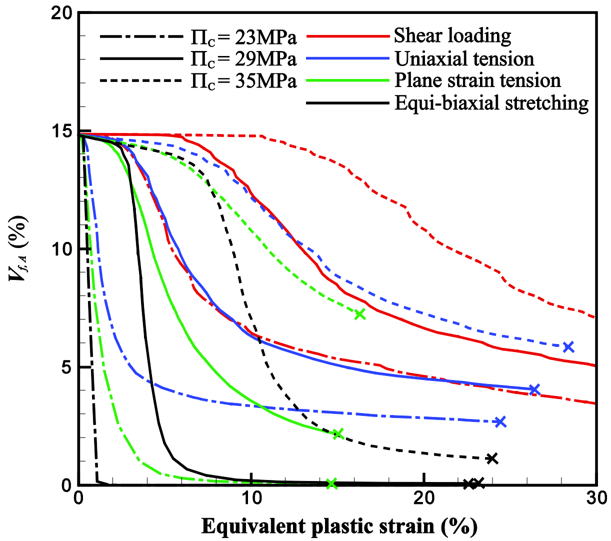

Austenite volume fraction for different loading conditions

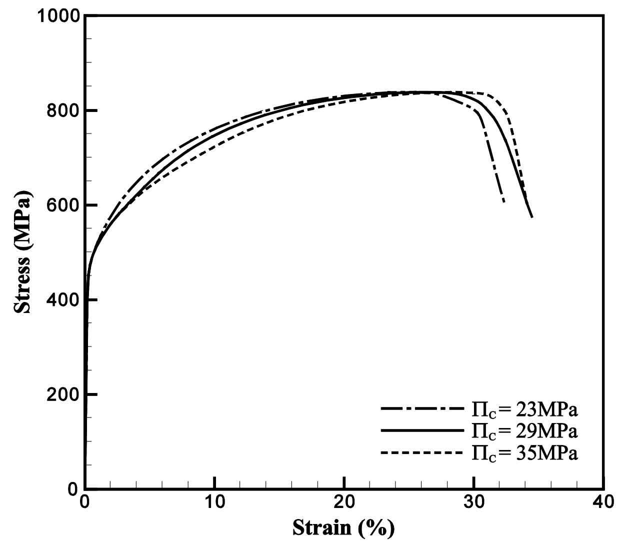

Overall response of the RVE

$$\Pi = R\sqrt{3J_2}\left[1 + k\frac{J_3}{J_2^{3/2}}\right] + \frac{\alpha I_1}{3}$$

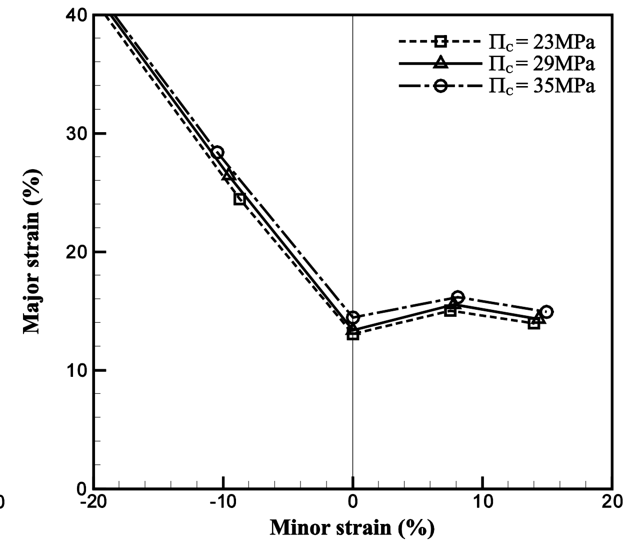

Pseudo-forming limit diagram

Choi, et al., Comp. Mat. Sci., 2011.

Prediction of Loading Path Dependency of FLD for AHSS

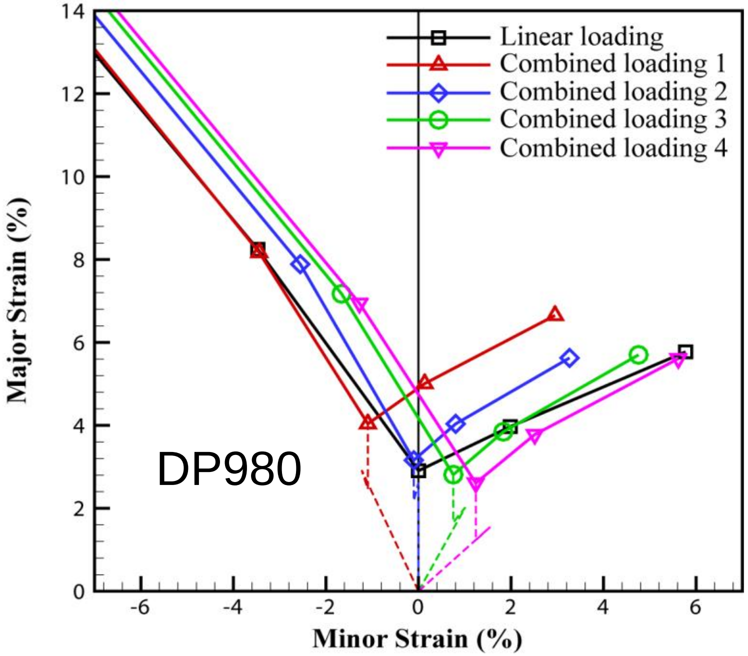

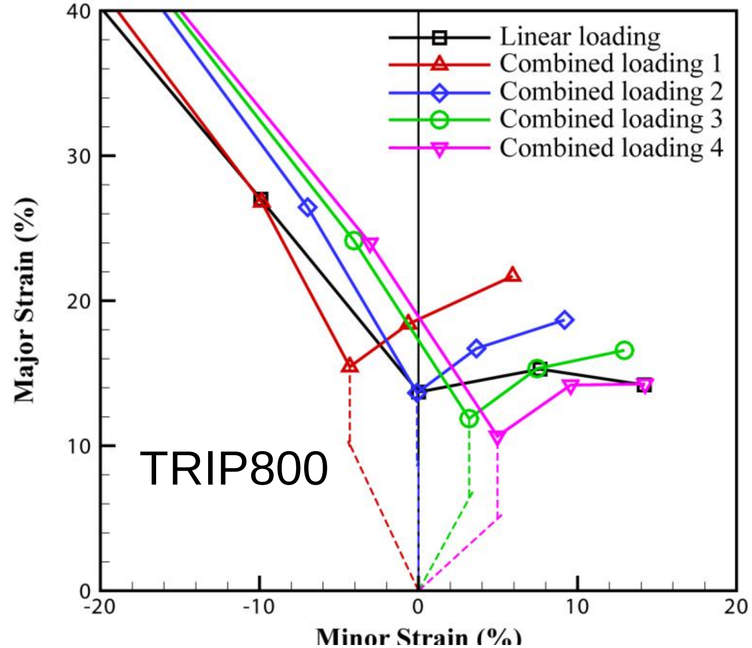

Strain-based

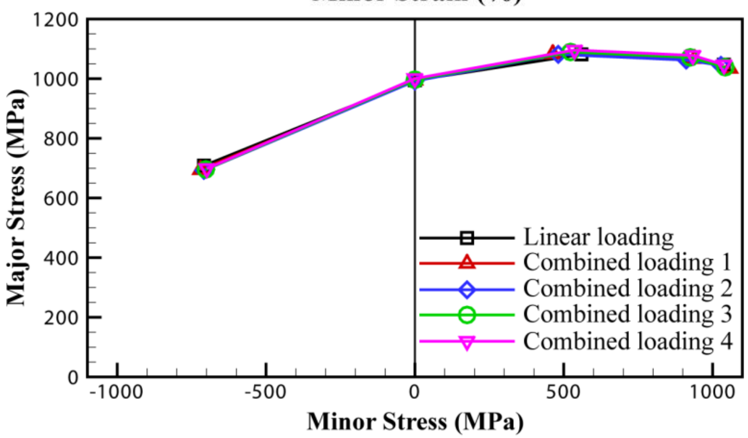

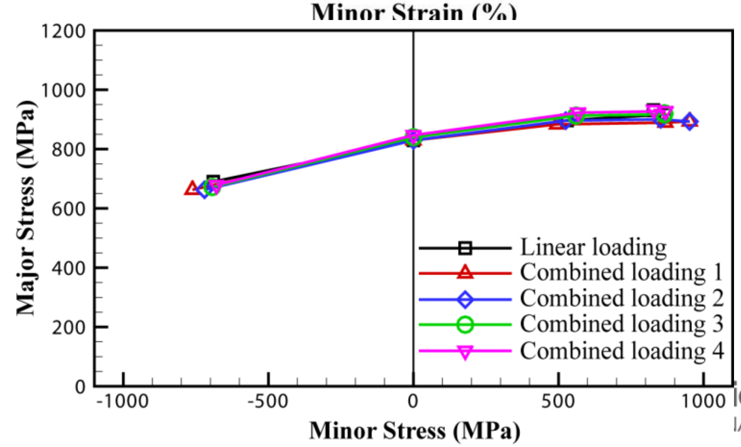

Stress-based

Choi, et al, Comp. Mat Sci., 2011, submitted.

Effects of Loading Rate on Tensile Ductility of TRIP800 Steel

- Dynamic stress versus strain curves needed for crash simulations of energy critical parts
  - Strength
  - Ductility
  - Energy absorption
- No national or international standards on dynamic tensile test
  - Set up
  - Sample design
  - Data acquisition
- Reported inconsistency in open literature, in particular for ductility of AHSS

Strain Rate Sensitivity of Ductility for IF Steels

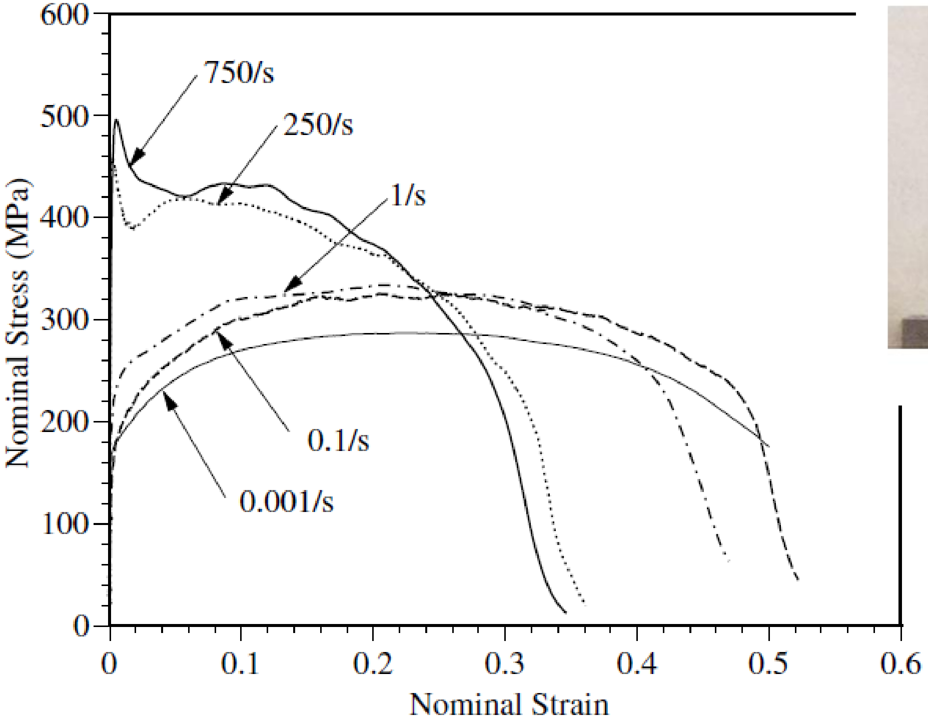

Fig. 4. Specimens after tensile tests at nominal strain rates of 750/s (left) and of 0.001/s (right).

Kuroda et al. *Int. J. Solid Struct*., 2006.
Mirza et al., J. Mat. Sci., 1996.

- Ductile to brittle transition: Ductility is significantly reduced at high strain rate:
  - Changes in the mobile dislocation density
  - Thermal softening

Strain Rate Sensitivity of DP600

- Inconsistent sample designs

Static

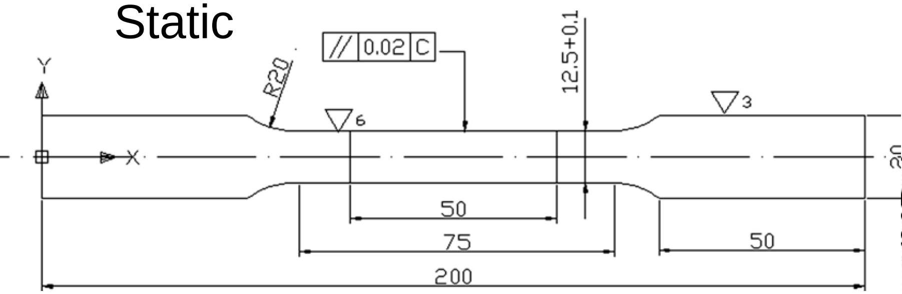

dynamic

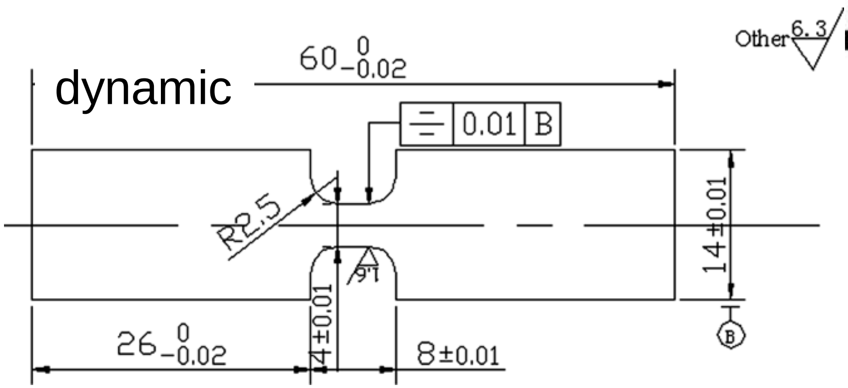

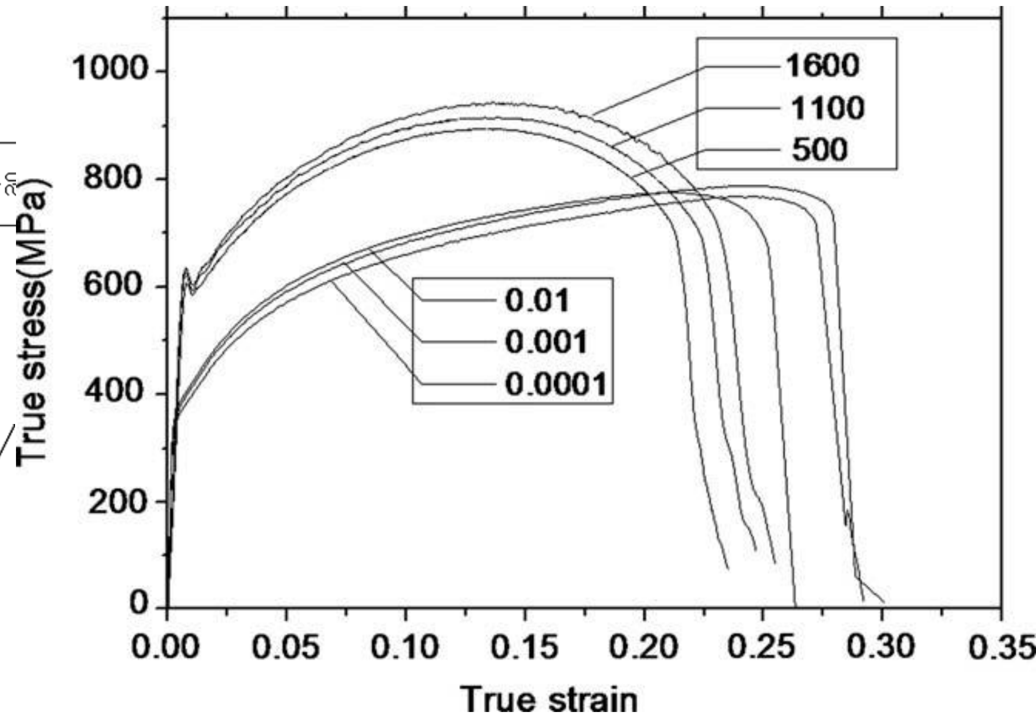

Yu et al. *Mat. And Design*, 2009.

Strain Rate Sensitivity of Ductility on TRIP700

- Mostly focused on strength and hardening behaviors
  - a gauge length *of 5mm and a radius of 1mm.*

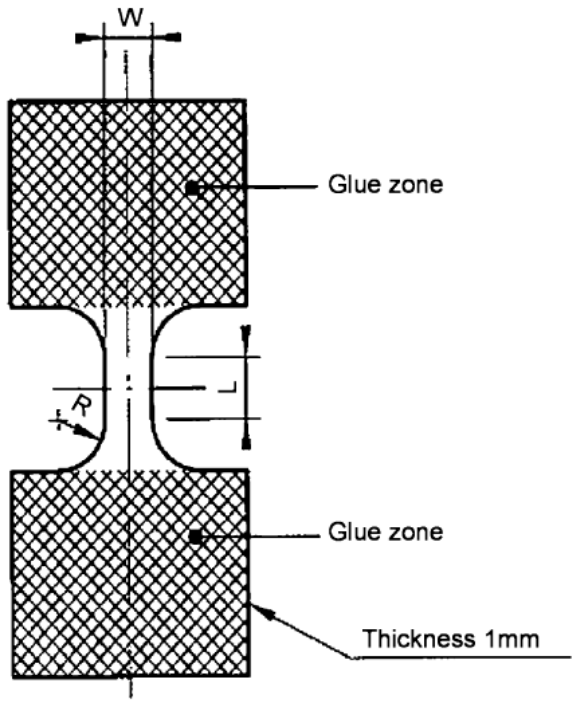

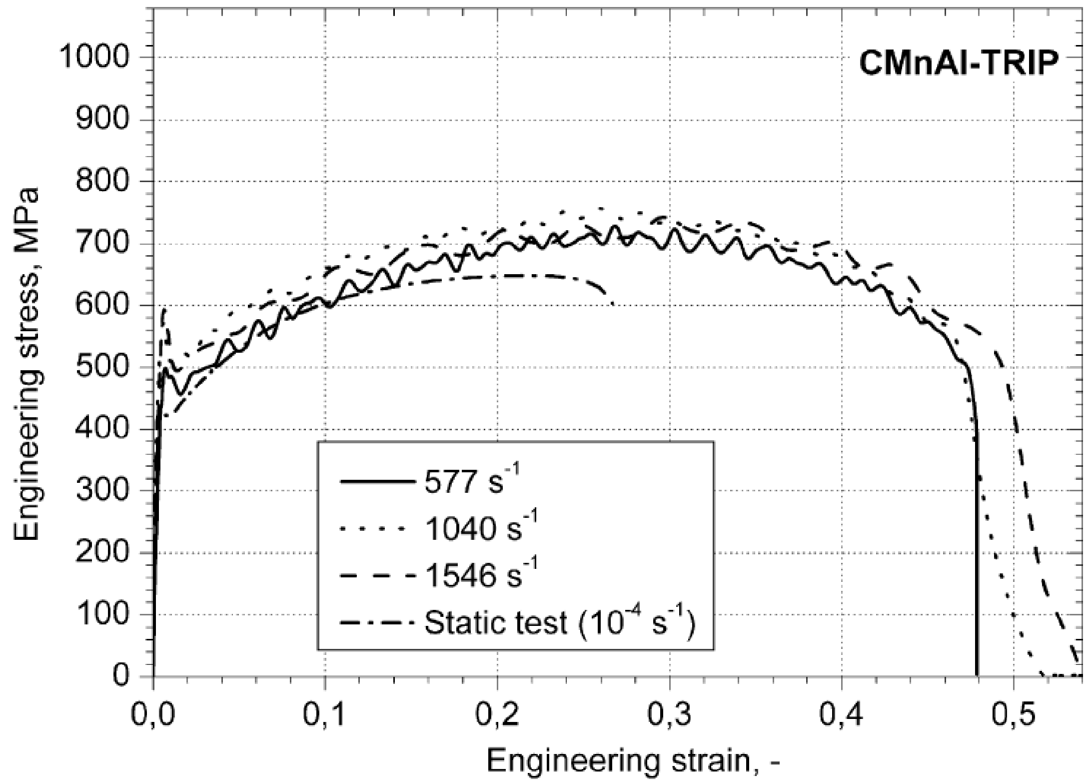

Van Slycken et al., Mat Sci Eng A 2007.

Experimental Procedures in This Study

- Quasi-static tensile test:
  - ASTM E-8 sub-sized sample
  - Miniature tensile sample
    - Displacement scaling
- Dynamic tensile test:
  - Kolsky tension bar test
  - Miniature tensile sample

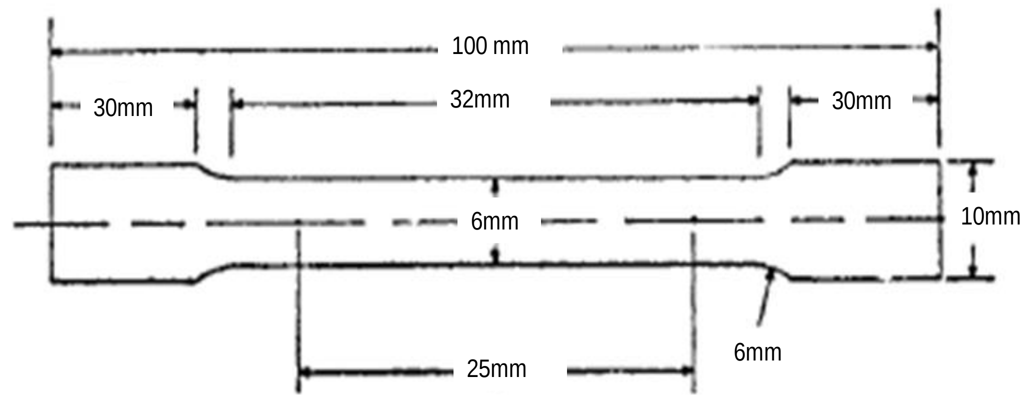

• Sun et al. *Mat. Sci. Eng. A*., in press 2011.

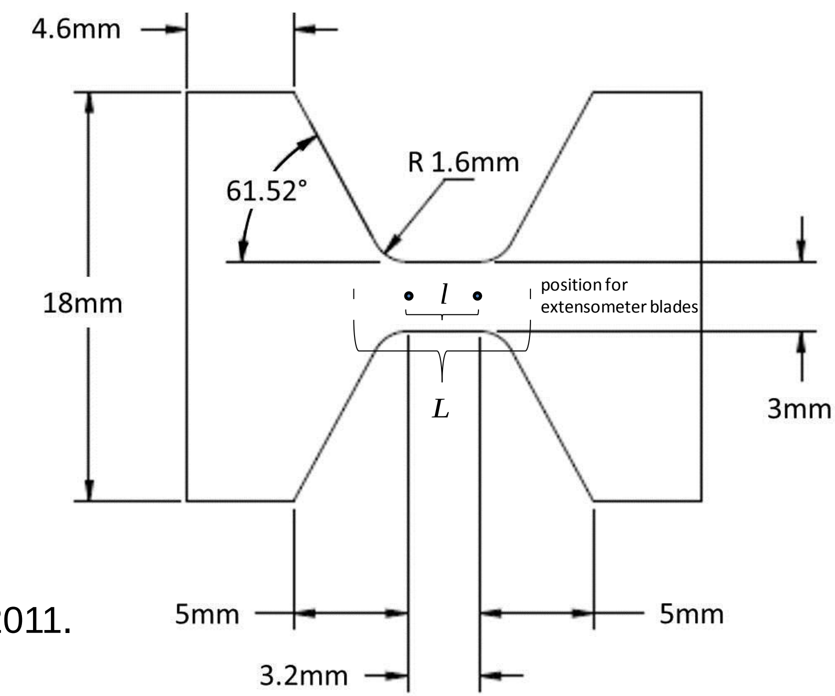

• Guzman et al., *Meas. Sci. Tech*., 2011.

Results on Geometry and Strain Rate Effects

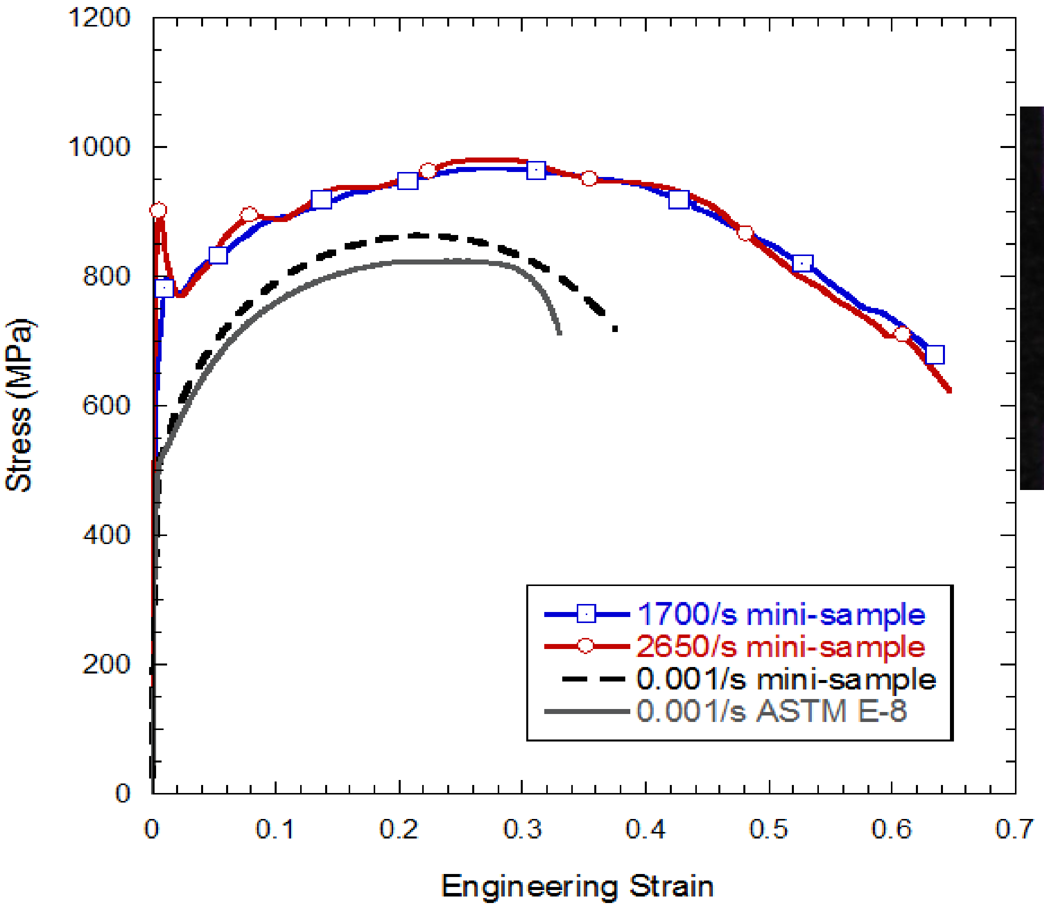

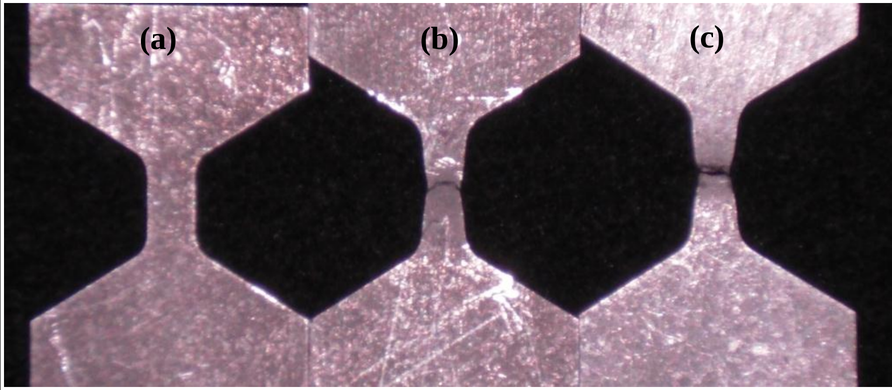

(a) Undeformed
(b) Quasi-static sample
(c) Dynamic sample

- Sun et al. *Mat. Sci. Eng. A*., in press 2011.

High Rate Deformation Mode Confirmed with High Speed Camera Images

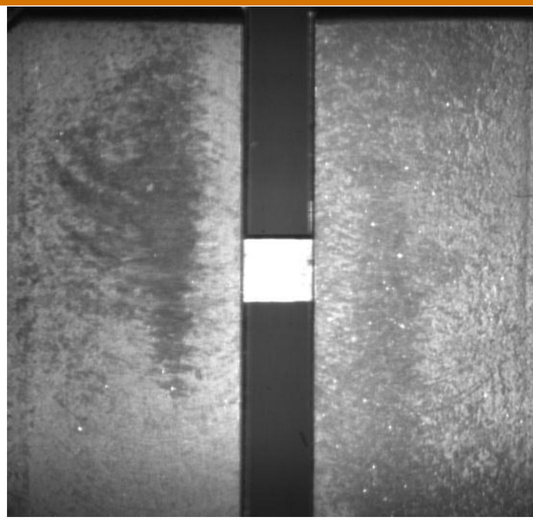

Frame 1: T = 0-microseconds 0% strain
(a)

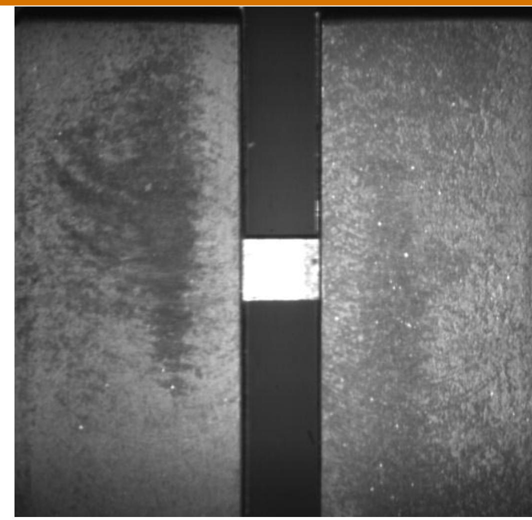

Frame 5: T = 105-microseconds 1% strain
(b)

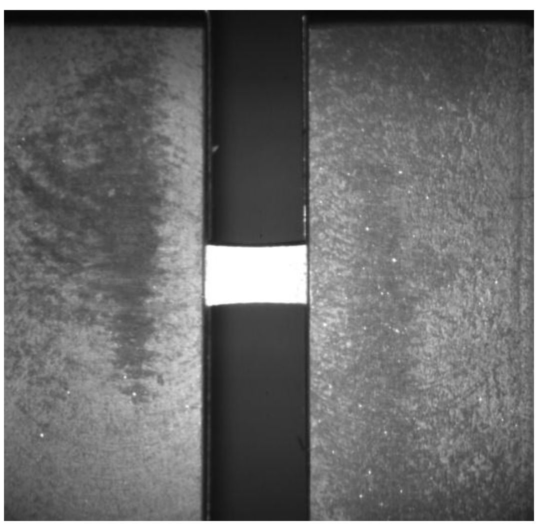

Frame 15: T = 315-microseconds 30% strain

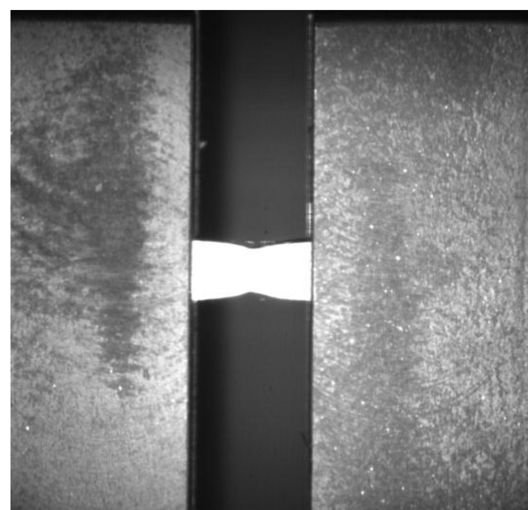

Frame 23: T = 480-microseconds 63% strain

Effects of Strain Rate on Ultimate Ductility

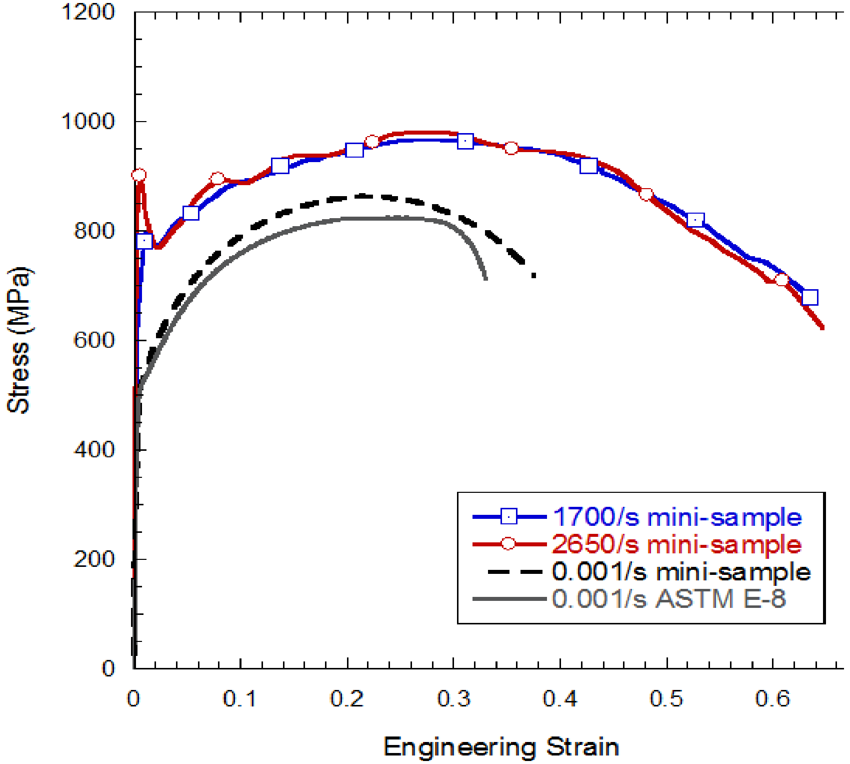

TRIP800

Sun et al. *Mat Sci. Eng. A*, in press 2011

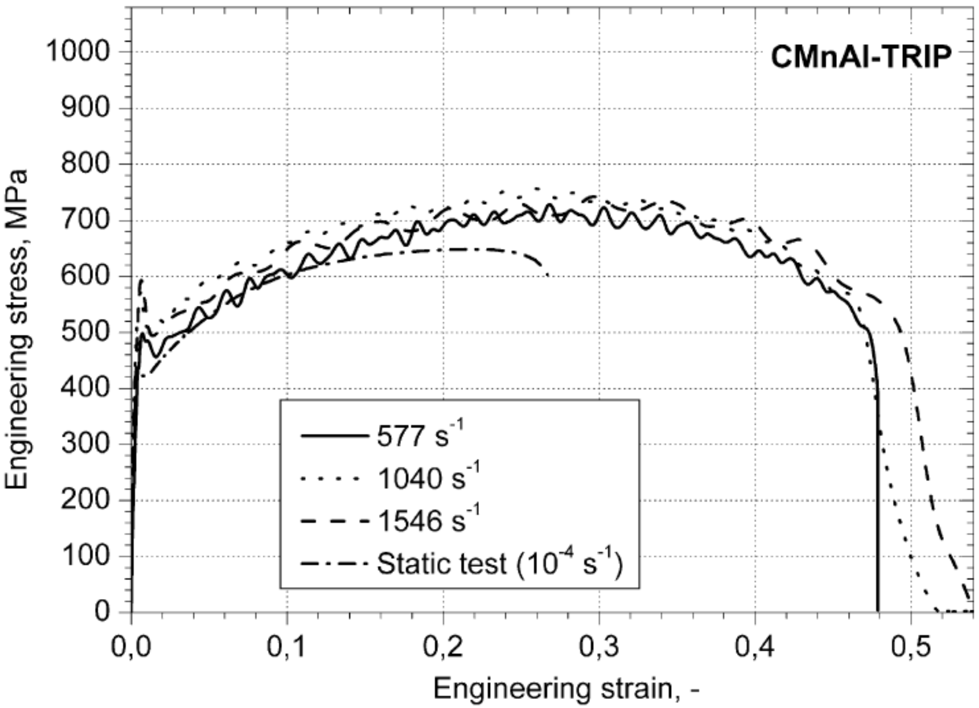

TRIP700

Verleysen et al., *Exp. Mech*. 2008.

Pacific Northwest NATIONAL LABORATORY

Proudly Operated by Battelle *Since 1965*

Possible Reasons for Enhanced Ultimate Ductility under High Rate Loading

- Inertial stabilization theory
  - Non uniform deformation suppressed by inertia at high strain rate
    - Shenoy and Freund, 1999
    - Seth et al., 2005
    - Why TRIP not IF steel?
- Adiabatic heating
  - Distributed nature of thermal softening
  - Grain elongation, rotation and alignment
  - Similar to high strain rate superplasticity of MMC?

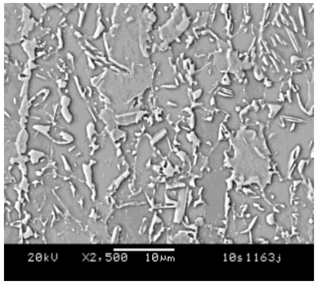

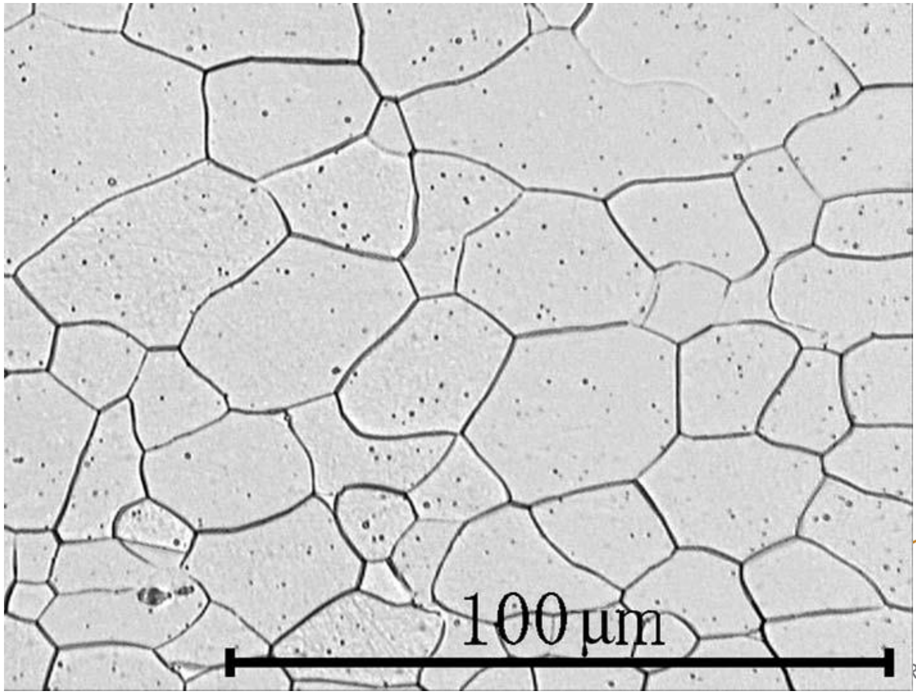

Adiabatic Heating at High Rate – Distributed vs. Localized

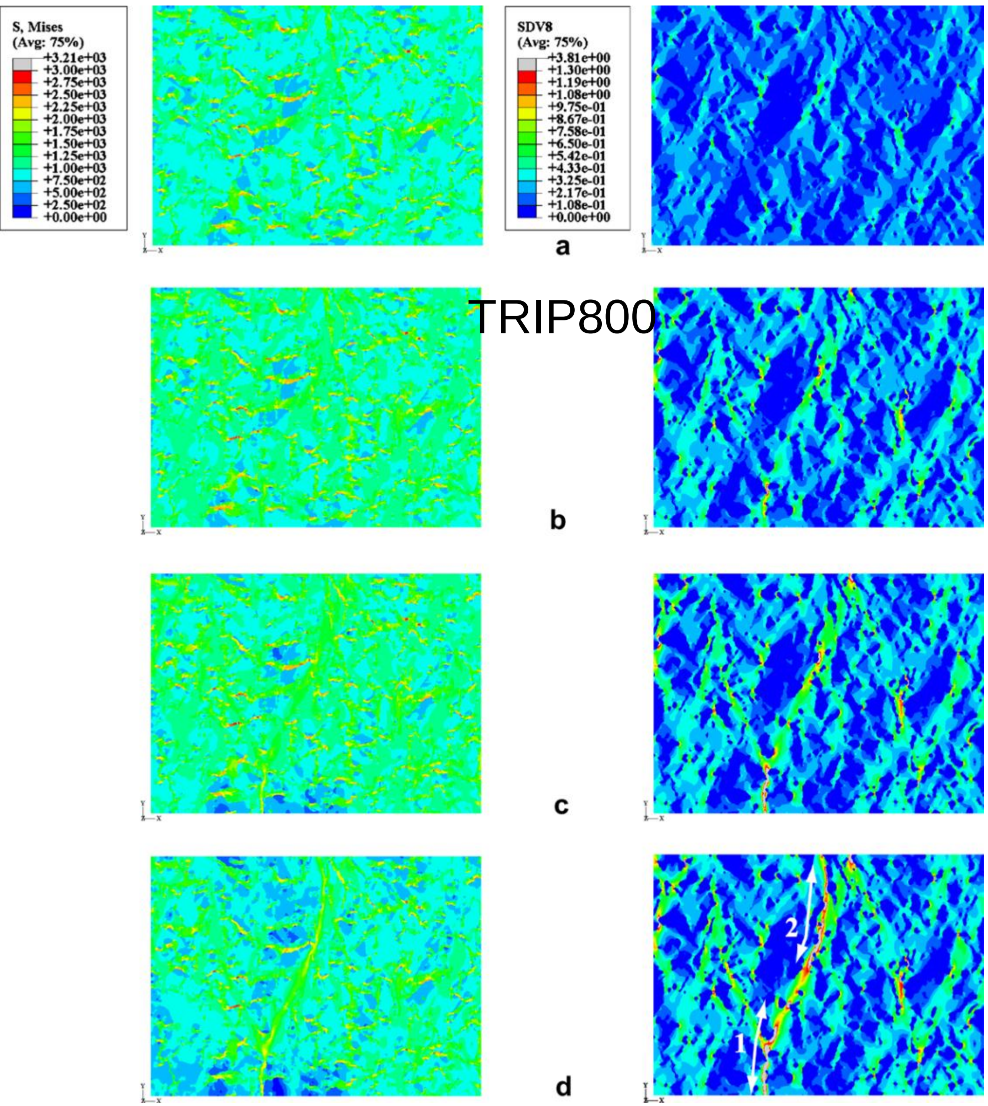

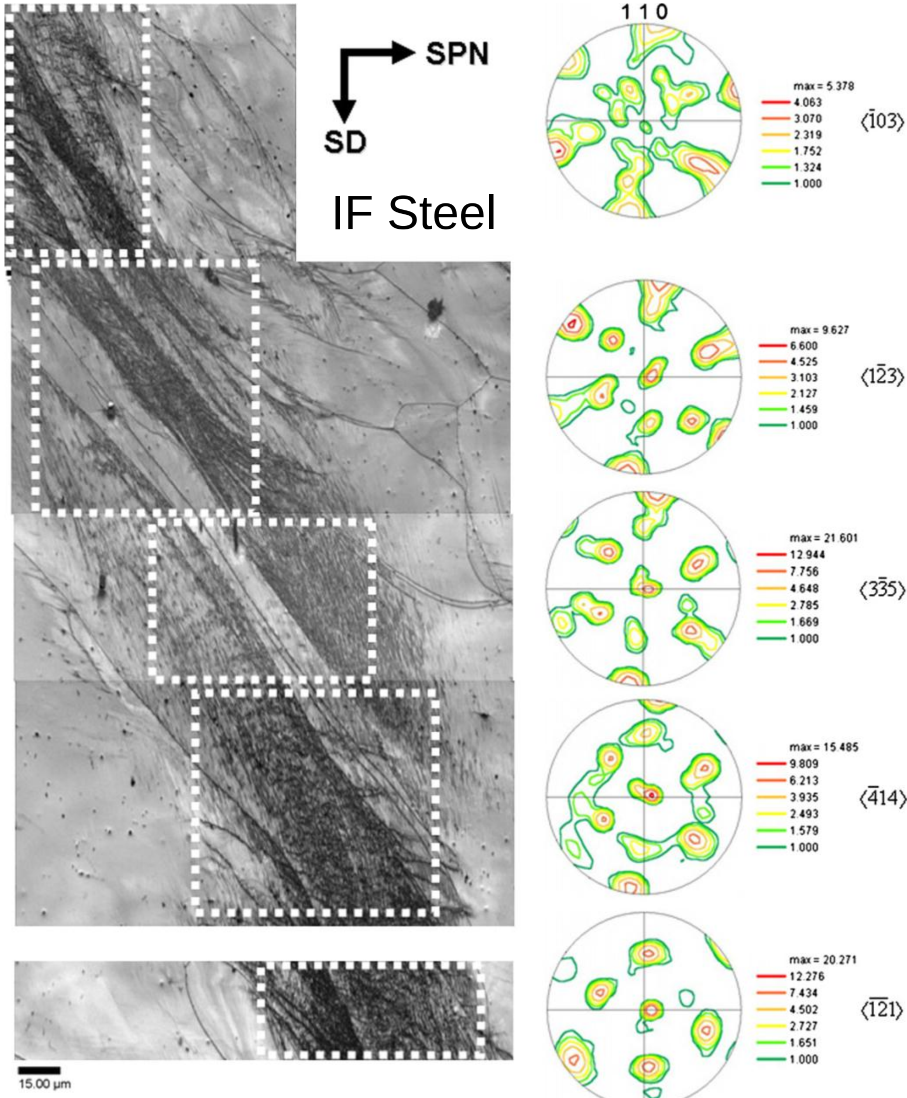

Lins, et al., Mat Sci. Eng. A, 2007.

Matrix Grain Rotation and Grain Boundary De-cohesion

Quasi-static

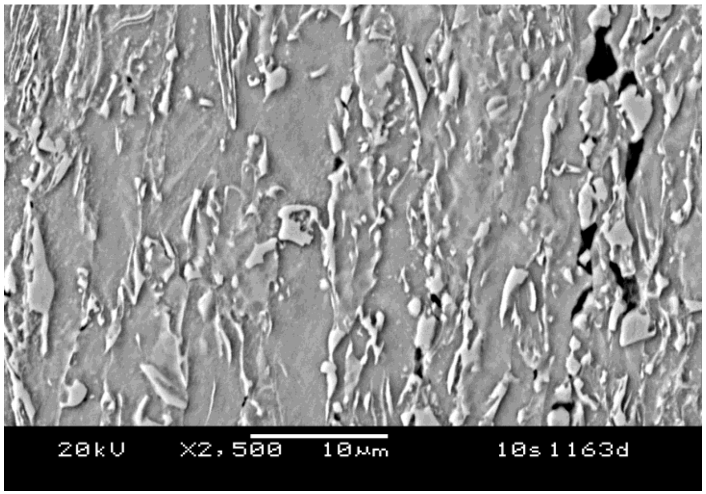

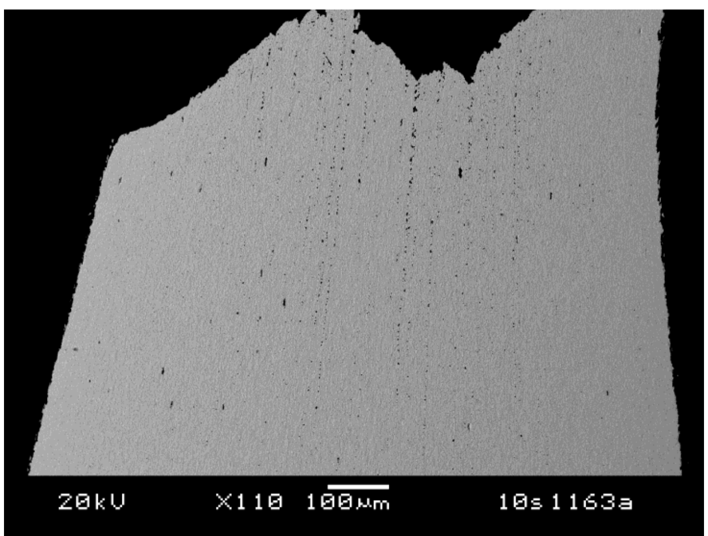

Dynamic

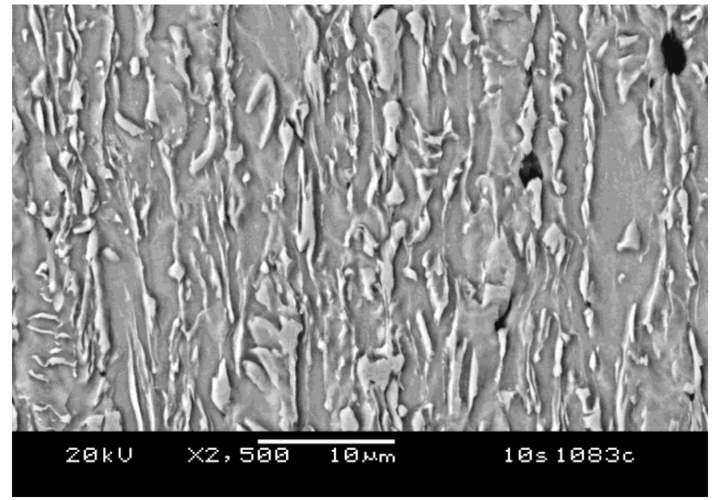

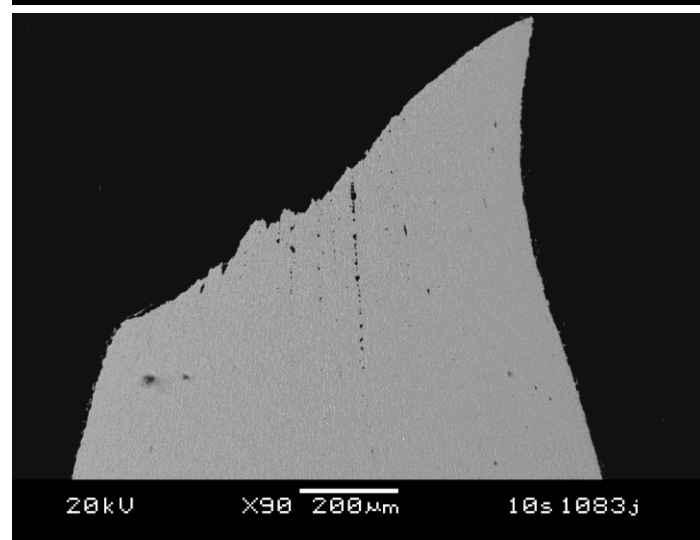

- Sun et al. *Mat. Sci. Eng. A*., in press 2011.

High Rate Localized Amorphism in ASB – TWIP

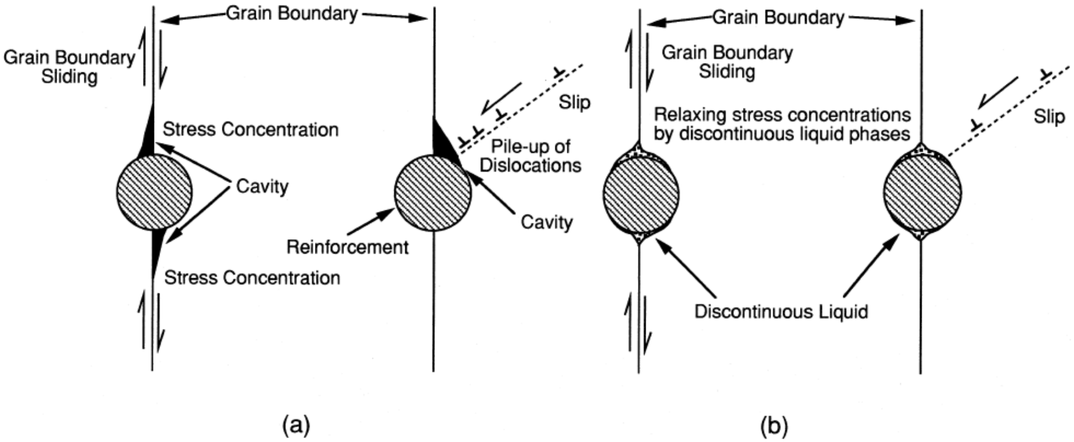

Fig. 2. Schematic illustrations of (a) cavity formation due to high stress concentrations at the interfaces and (b) relaxation of the stress concentrations by a liquid phase for metal matrix composites reinforced with particles.

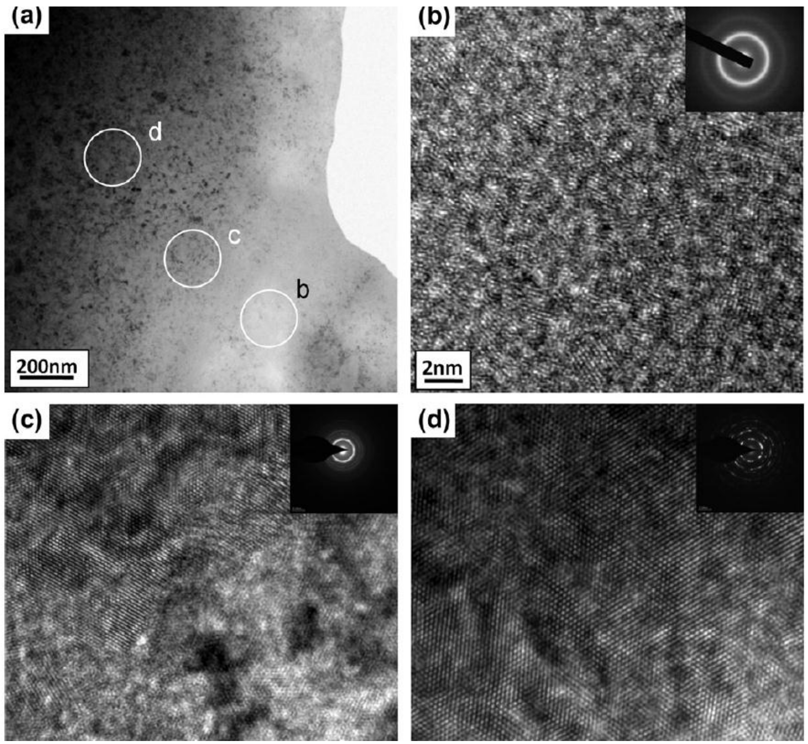

Mabuchi and Higashi, *Acta Mat*. 1999.

Li et al., *Acta Mat*. 2011.

Pacific Northwest NATIONAL LABORATORY

Proudly Operated by Battelle *Since 1965*

Shear Fracture: Ford and USS

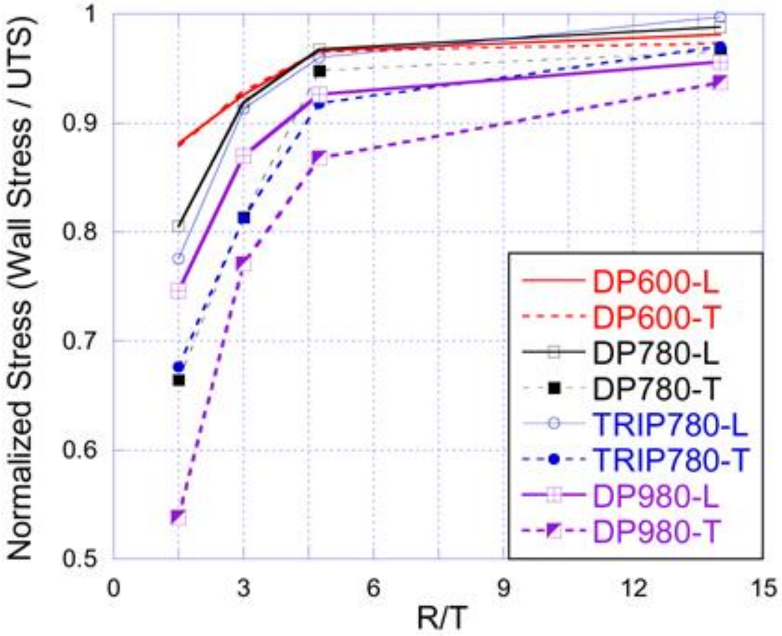

Shear fracture limit curves

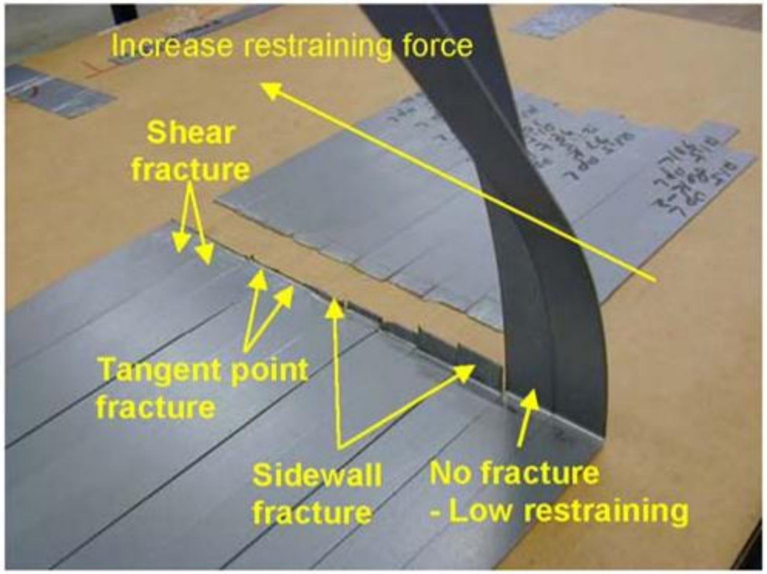

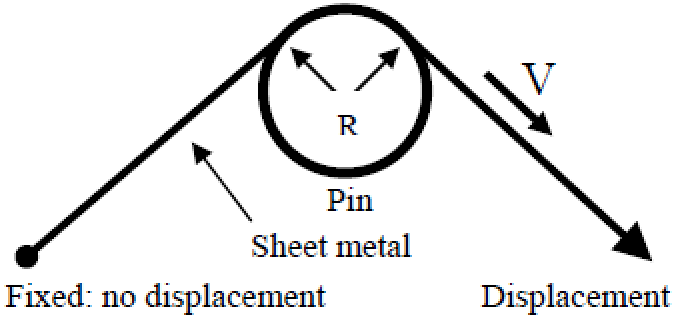

Shih, et al., MSEC2009-84070.
Zeng, et al., SAE 2009-01-1172.
Shih, et al., SAE 2010-01-0977.

Pacific Northwest
NATIONAL LABORATORY

Proudly Operated by Battelle *Since 1965*

PNNL Work on Local Formability

- Objectives
  - Identify the appropriate mechanical and microstructural properties that have significant influence on the local formability of DP980.
  - Develop appropriate screening method for local formability to promote wider application of AHSS
- Approach
  - Acquire different DP materials from various suppliers
  - Perform chemical composition analyses, microstructural analyses and various tests (Tension, HET, B-Pillar in-die stamping…) to obtain the mechanical properties for the obtained DP materials
  - Develop image analyses tools to quantify the grain size, volume fraction and aspect ratio…
  - Perform nano-indentation tests to determine the yield strengths of the constituent phases
  - Perform microstructure-based finite element analyses to gain to fundamental understandings on the key material features to withstand localized deformation
  - Derive a theoretical microstructure-to-properties correlations based on the results

Chemical Compositions

- Surface coating was removed before test
- Used ICP-AES and ASTM E1019-11

DP980 (t)	C (1.0)	D (1.2)	H (1.0)	G (1.4)	F (1.4)	A (2.0)	B (1.7)	E (2.0)
Al	0.05	0.05	0.03	0.04	0.04	0.03	0.04	0.03
C	0.11	0.12	0.15	0.08	0.10	0.09	0.09	0.09
Cr	0.26	0.25	0.32	0.47	0.47	0.02	0.20	0.46
Cu	0.01	0.01	0.04	<0.01	<0.01	0.07	0.01	<0.01
Mn	2.38	2.47	1.93	2.08	2.09	2.13	2.16	2.10
Mo	0.20	0.36	0.01	0.28	0.28	0.07	0.27	0.29
Ni	0.01	<0.01	0.04	0.01	0.01	0.01	0.01	0.01
P	0.008	0.014	0.010	0.008	0.007	0.007	0.008	0.008
S	0.003	0.004	<0.001	0.003	0.002	0.002	0.001	0.001
Si	0.08	0.03	0.64	0.18	0.18	0.57	0.31	0.33
Ti	0.04	<0.01	0.13	0.03	0.03	0.02	0.02	0.05
B	0.008	0.010	<0.002	0.008	0.008	0.003	0.008	0.008
Ca	<0.004	<0.002	<0.002	<0.002	<0.002	<0.002	<0.002	<0.002
Nb	0.031	0.002	0.003	0.017	0.017	0.009	0.015	0.036
V	<0.01	<0.01	<0.01	<0.01	<0.01	<0.01	<0.01	<0.01
Zn	<0.01	<0.01	<0.01	<0.01	<0.01	0.02	<0.01	<0.01
N	0.008	0.009	0.005	0.004	0.004	0.006	0.005	0.006

GOOD ← Formability ranking → BAD

Tensile Test (1)

- Tested ASTM E8 sub-size samples with $\dot{\varepsilon} = 10^{-4}$/sec
- Samples were cut by EDM from center and edge areas along rolling and transverse directions
- 3 tests for each condition

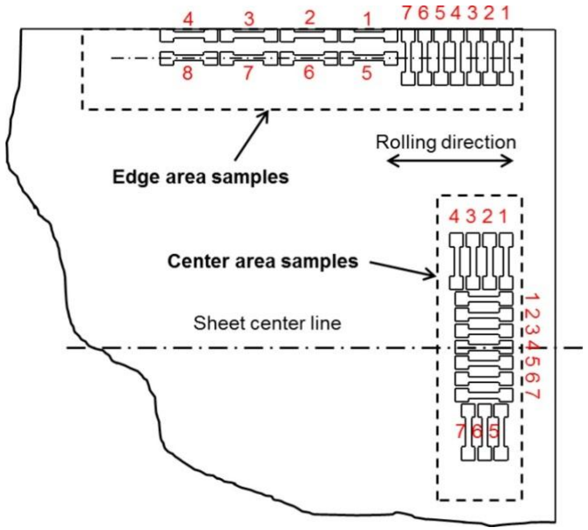

Sample Locations

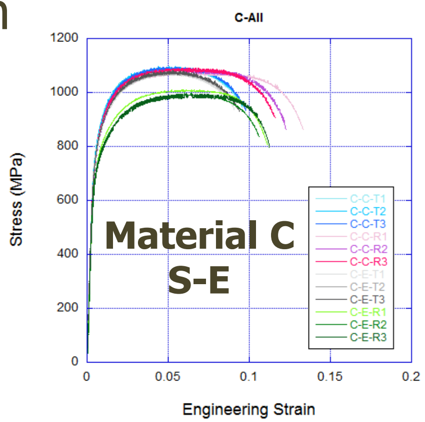

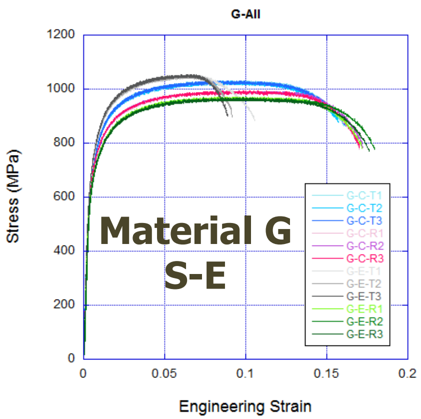

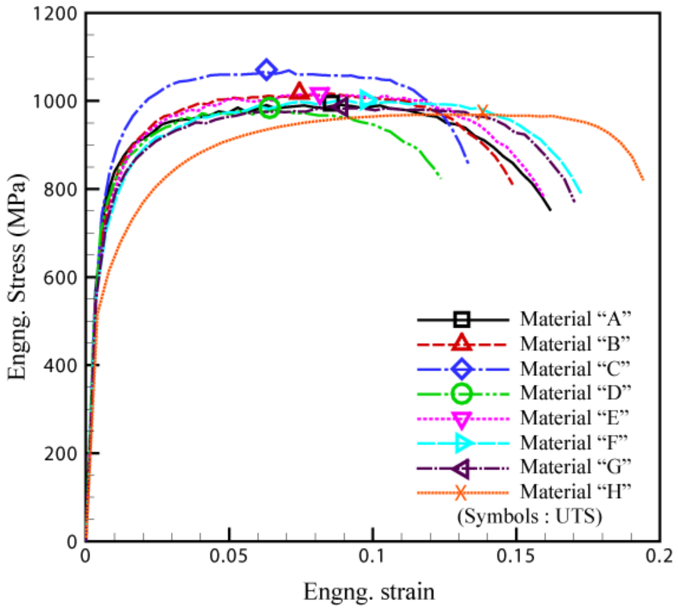

Comparison of S-E curves of DP980(Center/Rolling Dir.)

- S-E curves depend on sample location
- DP980 steels show large discrepancy in their performances
- See SAE 2012-01-0042 for S-E curves of other DP980

Microstructure Analysis (1) - SEM

- In-plane/through-thickness SEM pictures were obtained from surface and mid-thickness regions along rolling and transverse directions for center and edge areas
- Materials have different microstructures such as different size/shape of martensite grains and different distribution feature of martensite
- Different microstructural features were expected to induce different local formability → Image analysis

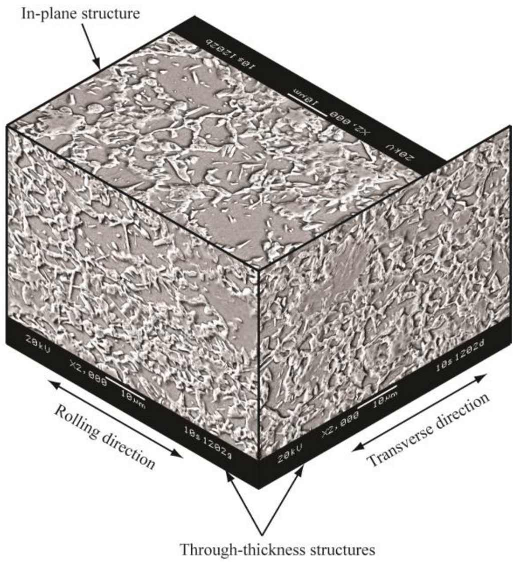

Material A

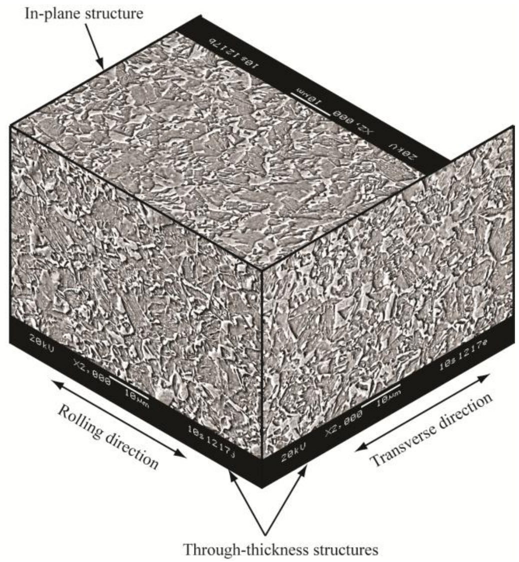

Material D

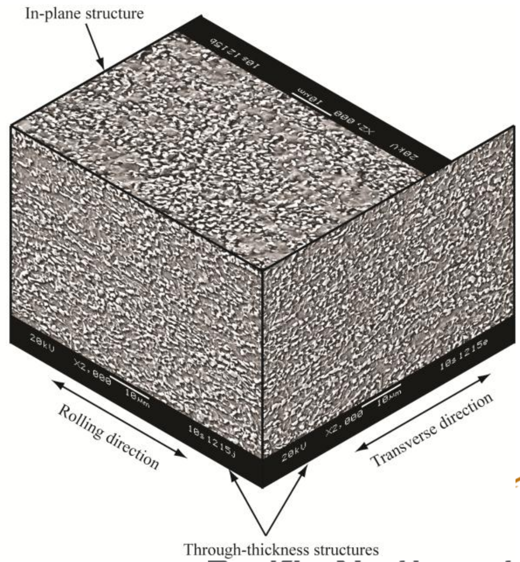

Material H

*See SAE 2012-01-0042 for more microstructures of other DP980

Channel Forming Test (1)

- Only 5 materials (C,D,F,G,H) were selected due to the allowable thickness limit of the forming die
- Square blanks (450mmX450mm) were formed using a straight rail die
- Lubricant was applied on the blank surface before forming
- Forming test was done both along the rolling and transverse directions

Successful forming

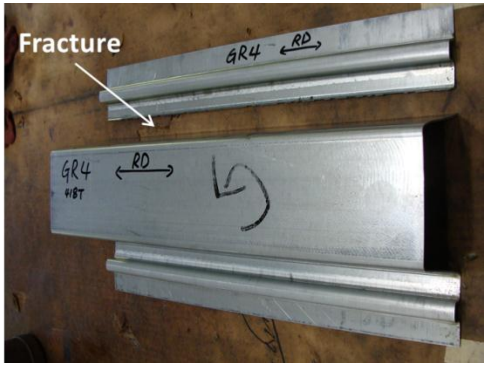

Fractured

Necking failure

Channel Forming Test (2)

- Forming test results

DP980 Thickness (mm)	Rolling Direction			Trans. Direction		
	No. of Trials	No. of Success	Success rate (%)	No. of Trials	No. of Success	Success rate (%)
C (1.0)	3	3	100	3	3	100
D (1.2)	4	3	75	3	3	100
F (1.4)	2	0	0	2	0	0
G (1.4)	4	2	50	3	1	33
H (1.0)	6	3	50	4	3	75

- Ranking of formability : **C > D > H > G > F**

Chemical Compositions

- Surface coating was removed before test
- Used ICP-AES and ASTM E1019-11

DP980 (t)	C (1.0)	D (1.2)	H (1.0)	G (1.4)	F (1.4)	A (2.0)	B (1.7)	E (2.0)
Al	0.05	0.05	0.03	0.04	0.04	0.03	0.04	0.03
C	0.11	0.12	0.15	0.08	0.10	0.09	0.09	0.09
Cr	0.26	0.25	0.32	0.47	0.47	0.02	0.20	0.46
Cu	0.01	0.01	0.04	<0.01	<0.01	0.07	0.01	<0.01
Mn	2.38	2.47	1.93	2.08	2.09	2.13	2.16	2.10
Mo	0.20	0.36	0.01	0.28	0.28	0.07	0.27	0.29
Ni	0.01	<0.01	0.04	0.01	0.01	0.01	0.01	0.01
P	0.008	0.014	0.010	0.008	0.007	0.007	0.008	0.008
S	0.003	0.004	<0.001	0.003	0.002	0.002	0.001	0.001
Si	0.08	0.03	0.64	0.18	0.18	0.57	0.31	0.33
Ti	0.04	<0.01	0.13	0.03	0.03	0.02	0.02	0.05
B	0.008	0.010	<0.002	0.008	0.008	0.003	0.008	0.008
Ca	<0.004	<0.002	<0.002	<0.002	<0.002	<0.002	<0.002	<0.002
Nb	0.031	0.002	0.003	0.017	0.017	0.009	0.015	0.036
V	<0.01	<0.01	<0.01	<0.01	<0.01	<0.01	<0.01	<0.01
Zn	<0.01	<0.01	<0.01	<0.01	<0.01	0.02	<0.01	<0.01
N	0.008	0.009	0.005	0.004	0.004	0.006	0.005	0.006

GOOD ← **Formability ranking** → BAD

Microstructure Analysis (2) – Image Analysis

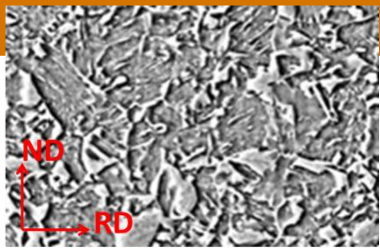

SEM of material D

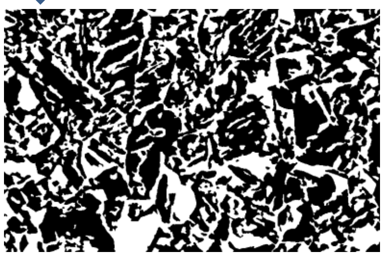

Binary image after image process

- Image processing tools are adopted to quantify several different microstructural features (i.e., volume fraction, average grain size/aspect ratio, average grain eccentricity, grain orientation etc.)
- Obtained quantity of microstructural features were compared with material's formability/ductility ranking
- Feasible correlations and trends between material microstructural features and its local formability could not be reasoned yet from any results of image analysis

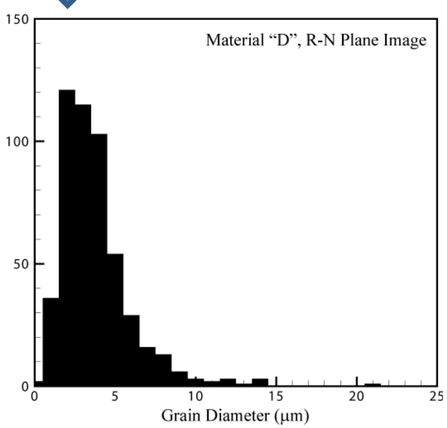

Histogram of martensite grain size

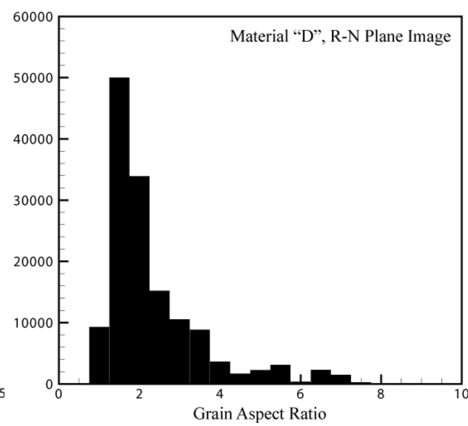

Histogram of martensite grain aspect ratio

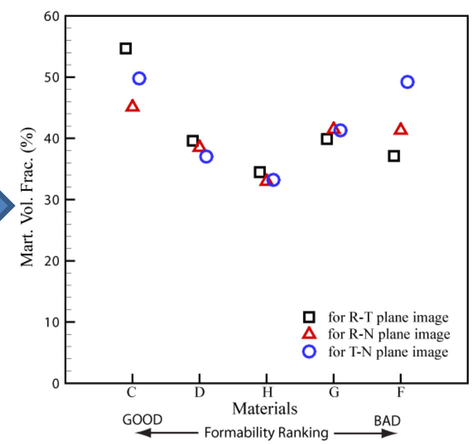

Martensite volume fraction in formability ranking

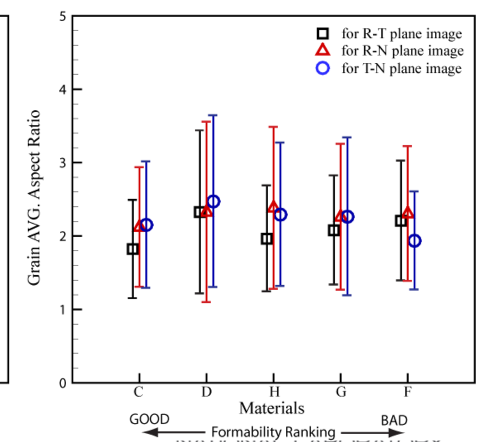

Martensite avg. grain aspect ratio in formability ranking

Tensile Test (2)

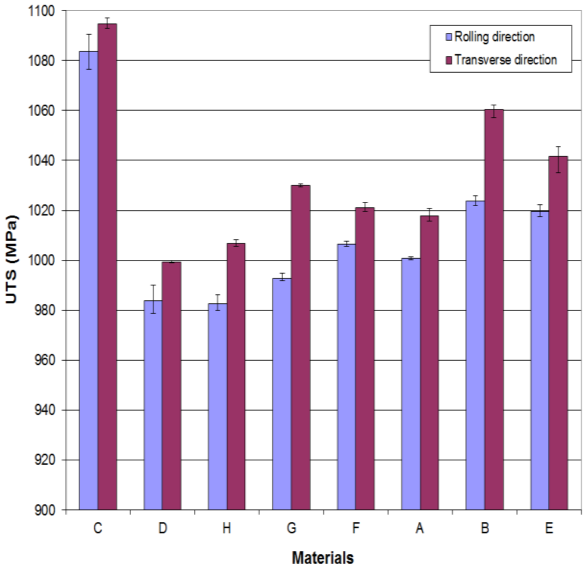

GOOD Formability ranking BAD

UTS vs formability ranking

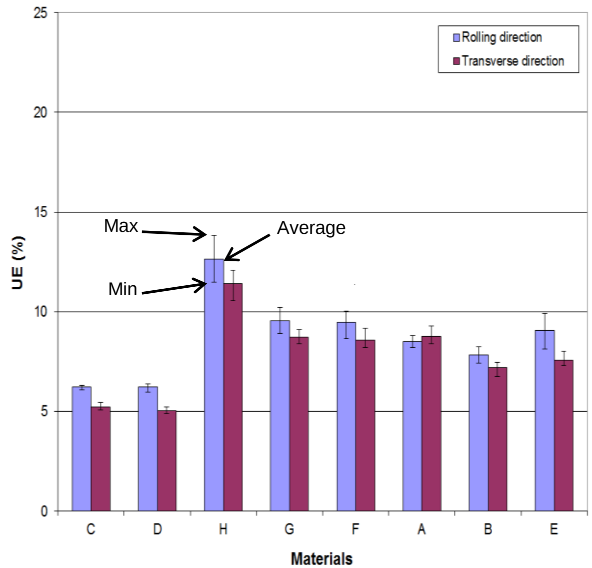

GOOD Formability ranking BAD

Uniform elongation vs formability ranking

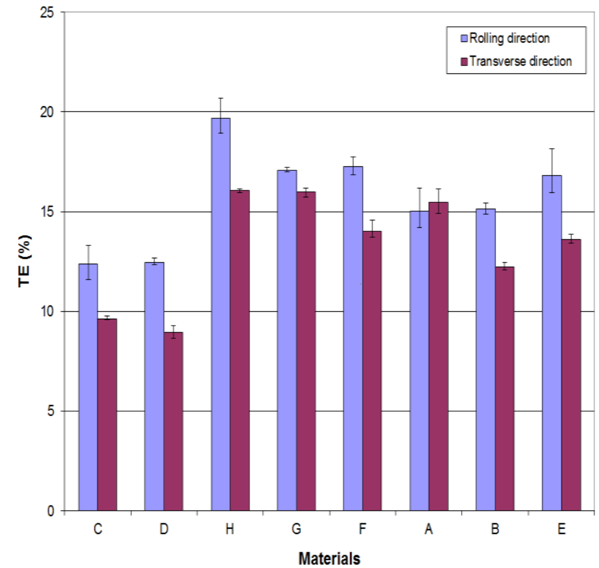

GOOD Formability ranking BAD

Total elongation vs formability ranking

- Some tensile properties (i.e., UTS, uniform elongation, total elongation) obtained from the center area samples were compared with formability ranking
- Correlation is not observed between tensile properties and local formability

Hole Expansion Test (1)

- Used square samples (75mmX75mm) with 12mm diameter hole
- Punch Dia.:40mm; Punch speed: 20mm/min; Die holding force: 100kN
- 2~3 tests were done for each material
- Holes were made with EDM and punching

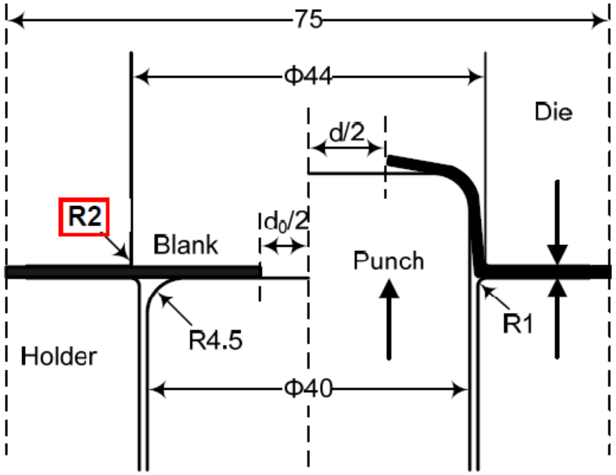

Schematic of HET

$$HER = \frac{d - d_0}{d_0} \times 100\%$$

Mat "C"

Mat "G"

EDM hole

Punch hole

Failed samples

Hole Expansion Test (2)

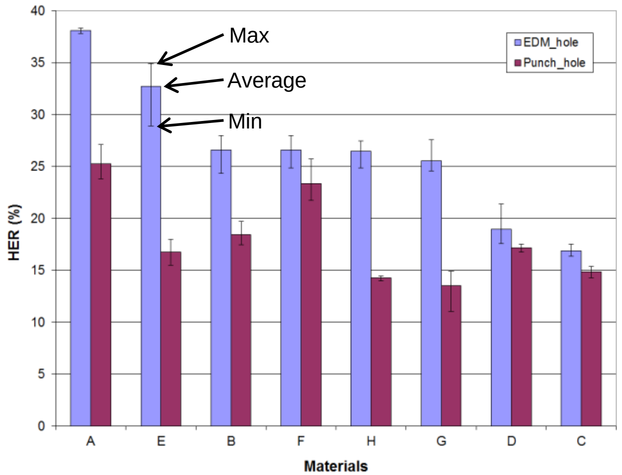

Comparison of HER
for different machining methods

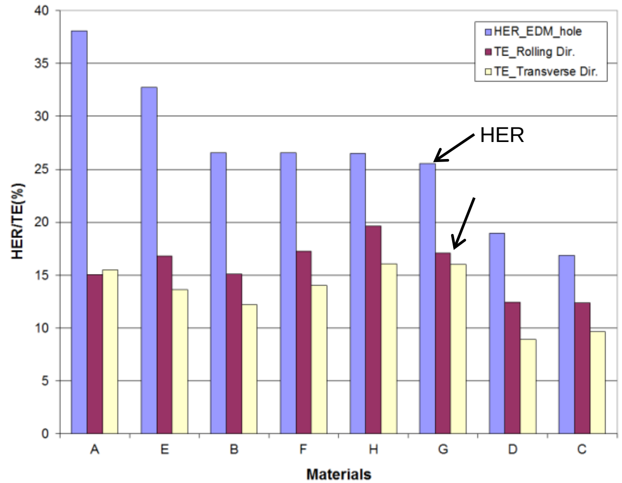

Comparison of HER of EDM
sample with total elongation

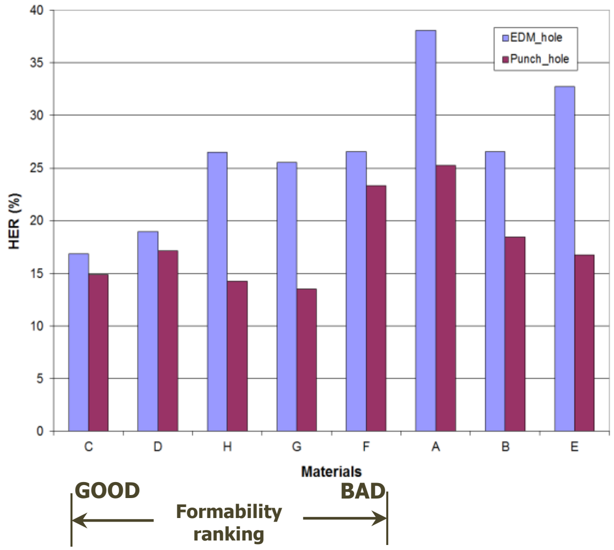

HER in formability ranking

- Correlation is not observed between the two different hole preparation methods: hole quality matters!
- HER does not necessarily correlate with total elongation (Thicker sheets appear to have higher HER)
- Correlation is not observed between HER and formability for both machining methods

Plastic Strain Ratio (r-value)

- Represents the resistance to thinning ($r = \varepsilon_w / \varepsilon_t$)
- Used ASTM E8 sub-size specimen and followed the manual procedure in ASTM E517
- 2 tests were done for each condition

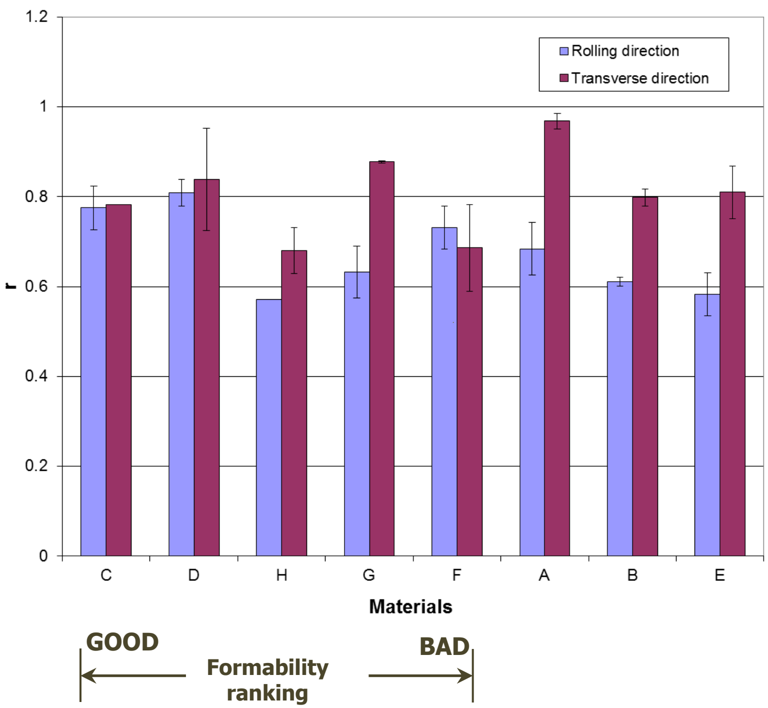

R-value in formability ranking

- It ‘appears’ that higher r-value is helpful to get better formability

Summary and Challenges

- Various tests have been performed with eight different DP980 steels to establish the fundamental understandings on key mechanical properties and the microstructure features influencing the local formability of AHSS
- Measured in-plane mechanical properties of these steels do not correlate with their local formability
- Image analysis was adopted for the SEM pictures of DP980 steels in order to quantify their various microstructural features
- It is not easy to find possible correlations between the microstructural features and the macroscopic deformation behaviors
- Nano-indentation test is underway to measure the strength disparity of the constituents
- Examinations of micro-damage near the cutting edge, induced from machining, is underway
- Larger-area microscopes may also be considered to examine the inhomogeneity of martensite distribution

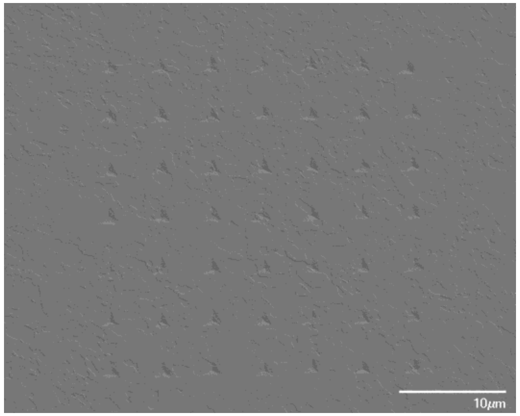

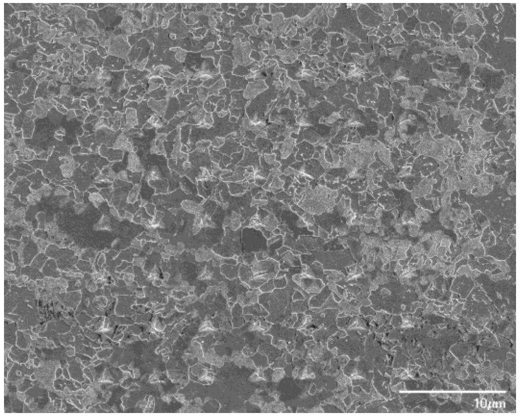

Preliminary nano-indentation test with material B

Can We Use the Micromechanics-Based FEM to Predict Localized Fracture?

- Experimental simulation of shear fracture
  - Stretch bending
- Two step plane strain simulation loading:
  - Stretching
  - Indentation
- Factors considered:
  - Initial stretching strain
  - Indenter radii

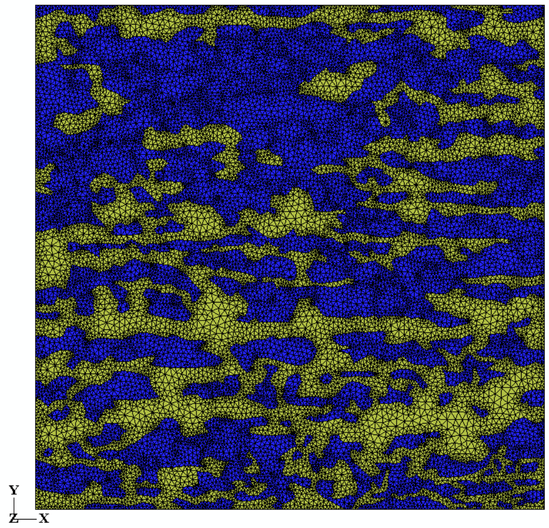

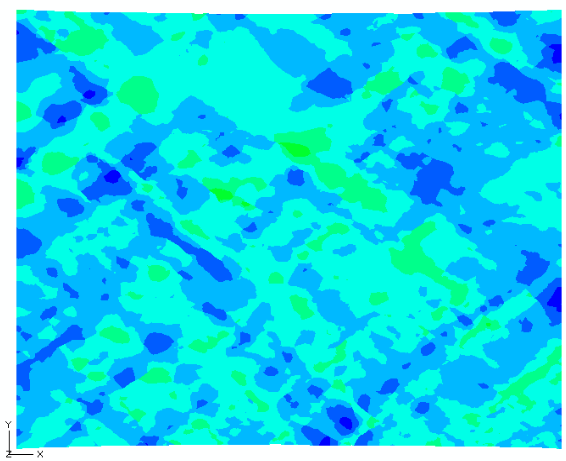

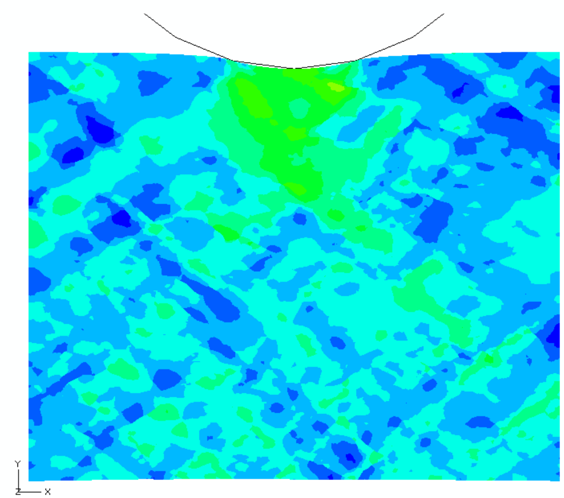

Effects of Indenter Radius and Indentation Location